2018

Microscale phase field modeling of the martensitic transformation during cyclic loading of NiTi single crystal

S. Ehsan Esfahani
Iowa State University, ehsan@iastate.edu

Iman Ghamarian
University of Michigan - Ann Arbor

Valery I. Levitas
Iowa State University, vlevitas@iastate.edu

Peter Collins
Iowa State University, pcollins@iastate.edu

Microscale phase field modeling of the martensitic transformation during cyclic loading of NiTi single crystal

Abstract
A microscale phase field model developed in Levitas et al. (2004) and Idesman et al. (2005) is slightly advanced for different and anisotropic elastic moduli of phases and is employed for the study of the stress-induced cubic-monoclinic phase transition in NiTi single crystal involving all 12 martensitic variants. The model is scale-independent, without the gradient term, and it is applicable for any scale greater than 100 nm. This model includes strain softening and the corresponding transformation strain localization, and it reproduces a discrete martensitic microstructure. The model only tracks finite-width interfaces between austenite and the mixture of martensitic variants, and does not consider the interfaces between martensitic variants. The model is implemented as a UMAT subroutine in a commercial finite element (FE) package, ABAQUS. Multiple problems for a uniaxial cyclic loading are solved to study the effect of mesh, strain rate, crystal orientation, different numbers of pre-existing nuclei, and the magnitude of the athermal threshold on the stress-strain responses as well as the microstructure evolution. The obtained results exhibit that the microstructure and global stress-strain responses are practically independent of mesh discretization and the applied strain rate for relatively small strain rates. While the presence of the initial nuclei in the sample decreases the nucleation stress, it slightly increases the total energy dissipation. The observed microstructure, the sudden drop in the stress-strain curve after initiation of the martensitic transformation, and the absence of a similar jump for the reverse phase transformation are in qualitative agreement with known experiments. Changing the crystallographic orientation of the sample varies the entire behavior, namely, the variants which are involved in the phase transformation, the morphology of the associated microstructure, the stress-strain curve, and the total dissipation. Athermal threshold, in addition to the expected increase in the magnitude of hysteresis, leads to some strain hardening for the direct phase transformation.

Keywords
Martensitic phase transition, NiTi, Strain softening, Microstructure

Comments
This is a manuscript of an article published as Esfahani, S. Ehsan, Iman Ghamarian, Valery I. Levitas, and Peter C. Collins. "Microscale Phase Field Modeling of the Martensitic Transformation During Cyclic Loading of NiTi Single Crystal." *International Journal of Solids and Structures* (2018). DOI: 10.1016/j.ijsolstr.2018.03.022. Posted with permission.

International Journal of Solids and Structures 000 (2018) 1–17

Contents lists available at ScienceDirect

International Journal of Solids and Structures

journal homepage: www.elsevier.com/locate/ijsolstr

Microscale phase field modeling of the martensitic transformation during cyclic loading of NiTi single crystal

S. Ehsan Esfahani [a], Iman Ghamarian [b], Valery I. Levitas [c,e,*], Peter C. Collins [d,e]

[a] Department of Aerospace Engineering, Iowa State University, Ames, IA 50011, USA
[b] Department of Materials Science & Engineering, University of Michigan, Ann Arbor, MI 48109, USA
[c] Departments of Aerospace Engineering, Mechanical Engineering, and Material Science & Engineering, Iowa State University, Ames, IA 50011, USA
[d] Department of Materials Science & Engineering, Iowa State University, Ames, IA 50011, USA
[e] Ames Laboratory, Division of Materials Science and Engineering, Ames, IA 50011, USA

ARTICLE INFO

Article history:
Received 18 October 2017
Revised 16 March 2018
Available online xxx

Keywords:
Martensitic phase transition
NiTi
Strain softening
Microstructure

ABSTRACT

A microscale phase field model developed in Levitas et al. (2004) and Idesman et al. (2005) is slightly advanced for different and anisotropic elastic moduli of phases and is employed for the study of the stress-induced cubic-monoclinic phase transition in NiTi single crystal involving all 12 martensitic variants. The model is scale-independent, without the gradient term, and it is applicable for any scale greater than 100 nm. This model includes strain softening and the corresponding transformation strain localization, and it reproduces a discrete martensitic microstructure. The model only tracks finite-width interfaces between austenite and the mixture of martensitic variants, and does not consider the interfaces between martensitic variants. The model is implemented as a UMAT subroutine in a commercial finite element (FE) package, ABAQUS. Multiple problems for a uniaxial cyclic loading are solved to study the effect of mesh, strain rate, crystal orientation, different numbers of pre-existing nuclei, and the magnitude of the athermal threshold on the stress-strain responses as well as the microstructure evolution. The obtained results exhibit that the microstructure and global stress-strain responses are practically independent of mesh discretization and the applied strain rate for relatively small strain rates. While the presence of the initial nuclei in the sample decreases the nucleation stress, it slightly increases the total energy dissipation. The observed microstructure, the sudden drop in the stress-strain curve after initiation of the martensitic transformation, and the absence of a similar jump for the reverse phase transformation are in qualitative agreement with known experiments. Changing the crystallographic orientation of the sample varies the entire behavior, namely, the variants which are involved in the phase transformation, the morphology of the associated microstructure, the stress-strain curve, and the total dissipation. Athermal threshold, in addition to the expected increase in the magnitude of hysteresis, leads to some strain hardening for the direct phase transformation.

Published by Elsevier Ltd.

1. Introduction

Shape memory alloys (SMAs) have been used widely in various applications ranging from minuscule tools in the biomedical industry to comparatively larger scale devices in automotive, aerospace, and civil engineering (Lagoudas, 2008). This is due to their exclusive thermo-mechanical properties exhibiting shape memory effect and pseudo-elasticity, with relatively large recoverable strains (e.g., up to 8% for NiTi) (Shaw and Kyriakides, 1995). The main deformation mechanism of SMAs is related to the stress-induced martensitic phase transformation between the high-temperature phase (austenite) and the low-temperature phase (martensite). The physical and mechanical properties of SMAs are influenced considerably by the evolution of the martensitic microstructure, which depends on the crystal and defect structures as well as external loadings (Jiang et al., 2016; 2017a; 2017b; 2017c). SMAs exhibit complex hysteretic stress-strain responses to the applied thermomechanical loadings. These responses are strongly affected by the microstructure. Therefore, obtaining a firm grasp of the controlling parameters affecting the microstructure evolution and mechanical properties brings the essence of finding proper modeling capabilities.

The superelastic behavior of SMAs at various temperatures and applied loading conditions has been explored experimentally (Shaw and Kyriakides, 1995; 1997a; He et al., 2010; Sun et al., 2012; Zhang et al., 2010). Macroscopic softening and localization

* Corresponding author.
E-mail address: vlevitas@iastate.edu (V.I. Levitas).

https://doi.org/10.1016/j.ijsolstr.2018.03.022
0020-7683/Published by Elsevier Ltd.

of deformation have been observed during the loading of SMAs (specifically NiTi) due to the material instability associated with the phase transformation (Iadicola and Shaw, 2004; Laplanche et al., 2017). Experiments exhibit a load peak (i.e., the nucleation stress), a stress drop in the macroscopic stress-strain response and a subsequent plateau (designated as a propagation stress) in the stress-strain curve during forward and reverse phase transformations (Shaw and Kyriakides, 1997a; Tobushi et al., 1993; Tse and Sun, 2000; Churchill et al., 2009). The strain softening behavior leads to the Lüders-like transformation-deformation bands in a sample, i.e., to a localized strain field within the transformed regions. Therefore, it is of great importance to find the evolution of discrete martensitic microstructure, which governs the macroscopic stress-strain response and internal stresses. This fact may cause damage and degradation of shape memory properties.

Different thermomechanical phenomenological and micromechanical models have been developed in Arghavani et al. (2010), Bo and Lagoudas (1999); Lagoudas et al. (2012), Lexcellent et al. (2000), Panico and Brinson (2007), Saleeb et al. (2011), Zaki and Moumni (2007), and Siredey et al. (1999) to study the martensitic phase transformation in SMAs. While it is prevailing that the microstructure evolution has a major impact on both macroscopic and microscopic properties of SMAs, the above models neglect the discrete martensitic microstructure. Instead, a smooth distribution of the volume fraction of martensite and (in some models) martensitic variants is used, which we will call a "smeared" description. Such a smeared description is a consequence of the strain hardening of the local constitutive equations, which prevents strain localization. In contrast, for discrete microstructure, the typical stationary solution consists of regions of complete martensite (volume fraction of martensite $c = 1$) and austenite (volume fraction of austenite $c_0 = 1$) divided by a finite-width transition region (interface).

A variety of models have been developed to study the heterogeneous strain field and discrete microstructure during the martensitic phase transformation. At the nanoscale, phase field or Ginzburg–Landau approach (Artemev et al., 2001; 2000; Levitas et al., 2010; Wang and Khachaturyan, 1997; Zhu et al., 2017) is generally employed to simulate the microstructure evolutions in materials. The evolution of phase transformation is determined by Ginzburg–Landau equations for the order parameters η_i. Special requirements for the transformation strain and the free energy have been introduced in Levitas and Preston (2002a,b), and Levitas et al. (2003), which in particular, results in zero derivatives of all interpolation functions for the austenite ($\eta_i = 0$) and the martensitic variant M_i (η_i). Further generalizations of this method have been attempted by including dynamics (Cho et al., 2012; Idesman et al., 2008), athermal threshold (Levitas and Lee, 2007; Levitas et al., 2010), large strains (Levin et al., 2013; Levitas, 2013), interfacial stresses (Levitas and Javanbakht, 2010; Levitas, 2014), and surface-induced nucleation (Levitas and Javanbakht, 2010; 2011). Although this approach is used extensively it is only applicable to the study of nanoscale samples. The problem is that the nanoscale phase field approach resolves the finite-width phase interface, which is on the order of 1 nm thick. Free energy includes the term involving gradient of the order parameter, which contains the scale parameter defining the interface width. The necessity of resolving the 1 nm thick interface by 4–5 finite elements or grid points to obtain a mesh-independent solution restricts the size of the sample in a range from 10^2 to 10^3 nm.

A microscale phase field approach was developed in Levitas et al. (2004) and Idesman et al. (2005), which was applied for the discrete martensitic microstructure evolutions in the specimen of a size larger than 100 nm and without an upper limit. In the model (Levitas et al., 2004; Idesman et al., 2005) the order parameter is the volume fraction of the martensite, which causes *strain softening (Fig. 1a) and material instability* during the phase transformation and the corresponding transformation strain localization (which reproduces a discrete martensitic microstructure). This is in contrast to phenomenological (Arghavani et al., 2010; Lagoudas et al., 2012; Lexcellent et al., 2000; Panico and Brinson, 2007; Zaki and Moumni, 2007) and micromechanical (Bo and Lagoudas, 1999; Saleeb et al., 2011) models, which include strain hardening and produce smeared description of martensite. Note that practically any of the models (Arghavani et al., 2010; Lagoudas et al., 2012; Lexcellent et al., 2000; Panico and Brinson, 2007; Zaki and Moumni, 2007; Bo and Lagoudas, 1999; Saleeb et al., 2011) can be transformed to a microscale phase field model and will reproduce discrete martensitic microstructure if one substitutes strain hardening with softening. The volume fraction of each martensitic variant is a traditional internal variable, which does not cause additional strain localization and formation of variant-variant interfaces. The key ingredient that produces the strain softening and transforms a traditional micromechanical model into a phase field model is the positive definite energy ψ_{in} of all interfaces and internal stresses, see Eq. (3). The model is practically scale-independent since a gradient term related to the surface energy is excluded. While majority of the phase field approaches include gradient energy, there are many exceptions. Thus, gradient energy was dropped in the phase field reaction-pathway approach to phase transformations (Denoual et al., 2010), dislocation evolution (Koslowski et al., 2002; Koslowski and Ortiz, 2004), and cavitation in liquid (Levitas et al., 2011), phase field microelasticity theory for modeling structurally inhomogeneities like voids, cracks, and polycrystalline aggregates (Wang et al., 2002), and elastoplastic phase field model (Guo et al., 2005). Since these models differ from traditional phase field models with gradient terms, most of them used some distinguishing name, like phase field microelasticity, elastoplastic phase field, etc. Model in Levitas et al. (2004) and Idesman et al. (2005) was called a microscale phase field model and we will keep this name as well.

To compensate for the lack of the gradient term the model implements the surface energy in an averaged sense by introducing the material coefficients in Helmholtz free energy. Formally, the model is still well posed due to its rate-dependence, similar to the viscoplastic regularization in shear banding (Beissel and Belytschko, 1996; Needleman, 1988). In practice the interface has a width of a single finite element, i.e., the solution is mesh-dependent. However, the preliminary results presented in Idesman et al. (2005) show that mesh-dependence is mostly concerned with the width of the interface, and it weakly affects the geometry of the entire martensitic microstructure and macroscopic stress-strain curves. Since the volume fraction is constrained between 0 and 1 there is no requirement for the derivative of the free energy and the transformation strain to be zero at the volume fractions equal to 0 and 1. For this reason, instead of complex Landau polynomials, the simplest linear mixture rule is used for all the material properties. This model was developed similarly to the phenomenological models for phase transformation but with strain softening during transformation instead of hardening (similar to elastoplastic models (Beissel and Belytschko, 1996; Shaw and Kyriakides, 1997a), which were used as ersatz models for the study of microstructure evolution). A more detailed micromechanical model which exhibits strain softening was developed in Levitas and Ozsoy (2009a,b) and implemented for finite element modeling of microstructure in Ozsoy and Babacan (2016). Alternatively, to increase the sample size within the Ginzburg–Landau approach, the width of the interface, δ, is increased artificially to $\sim 1\mu$m while keeping the correct expression for interface energy, E (Steinbach and Apel, 2006). This modification, of course, makes the distribution of stresses within the interface unrealistic, and strongly affects the distribution of order parameter.

Please cite this article as: S.E. Esfahani et al., Microscale phase field modeling of the martensitic transformation during cyclic loading of NiTi single crystal, International Journal of Solids and Structures (2018), https://doi.org/10.1016/j.ijsolstr.2018.03.022

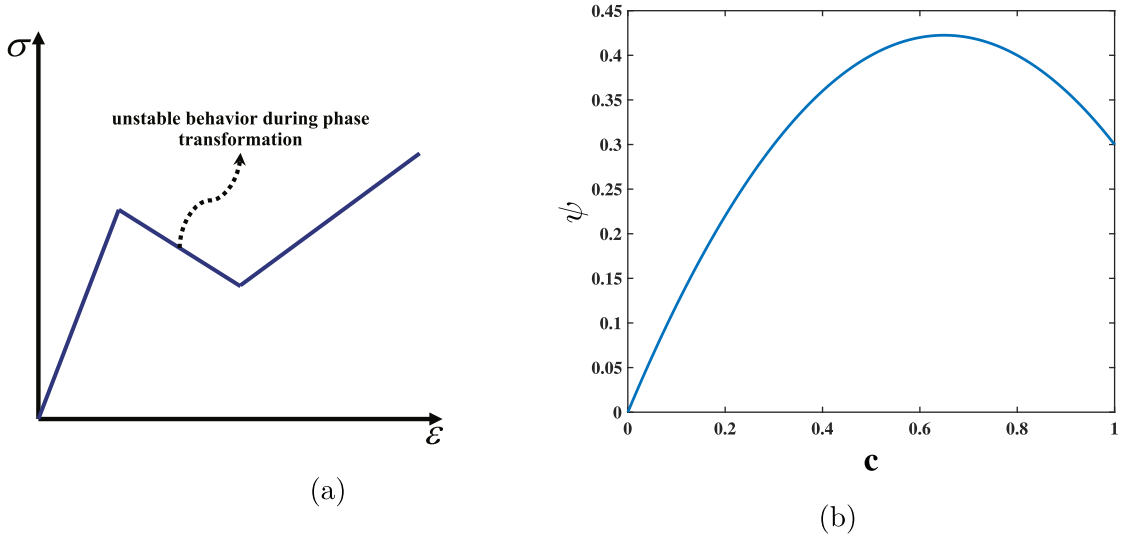

Fig. 1. Schematic local stress-strain diagram including a strain softening portion during phase transformation (a) and corresponding non-convex free energy versus the volume fraction of the martensite c (the order parameter) at fixed elastic strain (b).

In addition, since $E \sim \sqrt{A\beta}$ and $\delta \sim \sqrt{A/\beta}$, by excluding β we obtain $E \sim A\delta$, where A is the magnitude of the double-well barrier and β is the gradient energy coefficient (e.g., Levitas et al., 2003). Thus, the artificial increase in δ at fixed E leads to the decrease in the barrier, A, with the same proportion. Since A is determining the temperature and the stress for homogeneous nucleation as well as the stress hysteresis, increasing δ (reducing A) by a factor of 1000 will practically lead to a barrierless nucleation for both phases, drastic changes in macroscopic stress-strain curves (Levitas and Preston, 2002a; 2002b; Levitas et al., 2003), and multiple artificial nucleations during the simulations due to a stress heterogeneity. Note that while in nanoscale phase field approach the interface represents a smooth transition between two crystal lattices, in the larger-scale phase field approach an interface is a mixture of austenite and martensite variants. Based on the assumed geometry of phases in the mixture and some additional requirements, various homogenization schemes have been developed for the description of effective properties of interfaces (Mosler et al., 2014; Schneider et al., 2015).

In some models the total strain components are considered as order parameters, and strain gradient is included in the free energy (Barsch and Krumhansl, 1984; Falk, 1983; Jacobs, 1992; Chang et al., 2006; He and Sun, 2010). Some problems arise in this approach due to the impossibility to describe constant (stress and temperature independent) transformation strain and the required stress-strain response, as well as due to an insufficient number of material parameters to include all material properties of the austenite and martensite even in one-dimensional loading, see (Levitas and Preston, 2002a).

In the current study, a slightly extended version of a scale-independent phase field model developed in Levitas et al. (2004) and Idesman et al. (2005) is used to study the superelastic behavior of NiTi and the multivariant martensitic microstructure evolutions during the loading/unloading of a single crystal NiTi. The difference with Levitas et al. (2004) and Idesman et al. (2005) is in applying different elastic moduli of the austenite and martensite and anisotropic elasticity for both cubic and monoclinic lattices of the austenite and twelve martensitic variants of NiTi only. From a computational point of view, treating twelve variants for cubic to monoclinic transformation is more challenging for convergence and computational time than considering two of three variants for cubic to tetragonal transformation in Levitas et al. (2004) and Idesman et al. (2005). In this study two key questions in particular will be addressed:

(a) Since the model is scale-independent, can inherent mesh dependence be mitigated and a practically mesh-independent solution be obtained?
(b) Due to the linear kinetic relationship between the rate of volume fraction of martensitic variants and the thermodynamic net driving forces for the transformations the model is expected to be time-, and consequently, strain rate-dependent. While some strain rate dependence of the SMA response is observed in experiments (Zhang et al., 2010; Nemat-Nasser and Choi, 2005) it is usually related to thermoelastic heating which changes transformation stress. Since temperature variation is neglected here it is desirable to obtain a strain rate-independent response.

This paper is organized as follows. The phase field model is described in Section 2. Problem formulation and material properties are described in Section 3. Solutions of various problems on uniaxial cyclic loading of NiTi single crystals are discussed in Section 4. Thus, the effects of mesh, strain rate, crystal orientation, different numbers of pre-existing nuclei, and the magnitude of the athermal threshold on the stress-strain responses and microstructure evolution are studied. The obtained results, in particular, demonstrate that the microstructure and global stress-strain responses are practically independent of discretization mesh and of the strain rate for relatively small strain rates. Concluding remarks are presented in Section 5.

In this paper, vectors and tensors are designated in bold; $\boldsymbol{A} \cdot \boldsymbol{B}$ and $\boldsymbol{A}: \boldsymbol{B}$ represent respectively the contraction and double contractions of two tensors; subscript s designates the symmetric part of the tensor.

2. Description of the model

The key point in the formation of the discrete martensitic microstructure is to develop a model which exhibits an unstable region in the local stress-strain curve (Fig. 1a), similar to the usual phase field or Ginzburg–Landau models (Levitas and Preston, 2002a; 2002b; Levitas et al., 2003). The strain softening during phase transformation is responsible for the transformation strain localization and formation of fully transformed martensitic regions, separated from austenite by finite width interfaces. This is

contrary to well-known phenomenological approaches (Arghavani et al., 2010; Bo and Lagoudas, 1999; Lagoudas et al., 2012; Lexcellent et al., 2000; Panico and Brinson, 2007; Saleeb et al., 2011; Zaki and Moumni, 2007) that provide a smeared distribution of the volume fraction. The phase field model for a general case of multivariant martensitic phase transformation in elastic materials developed in Levitas et al. (2004) and Idesman et al. (2005) is advanced and described. A representative volume with the size of 100 nm or larger is considered which includes a sufficient number of m martensitic variants and austenite.

Here $\boldsymbol{u}$ is the displacement vector and $\boldsymbol{x}$ is the position vector. In the current paper the subscript 0 always denotes austenitic phase, and c_0 and c_i are the volume fractions of austenite and the ith martensitic variant, respectively, and $c = \sum_{i=1}^{m} c_i$ is the volume fraction of martensite. Thus, $c_0 + \sum_{i=1}^{m} c_i = 1$. The macroscopic transformation strain, $\boldsymbol{\varepsilon_t}$, can be calculated according to Eq. (6), where $\boldsymbol{\varepsilon_{ti}}$ indicates the Bain strain tensor for the transformation of a crystal lattice of austenite to the ith martensite variant. The rate of change of the volume fraction of the variant i can be expressed in terms of the rates $\dot{c}_{ij}$ of transformation from variants M_j to the variant M_i with the help of Eq. (7). The Hooke's law can be presented by Eq. (8), where $\boldsymbol{\sigma}$ is the stress tensor, $\boldsymbol{E}$ is the fourth-rank tensor of effective elastic moduli (see (9)), $\boldsymbol{E}_0$ and $\boldsymbol{E}_i$ are the tensor elastic moduli of the austenite and ith martensitic variant, respectively.

The Helmholtz free energy is accepted in the following form

$$\psi(\boldsymbol{\varepsilon_e}, c_i, \theta) = \psi_{el}(\boldsymbol{\varepsilon_e},\ c_i) + c_0\psi_0^{\theta}(\theta) + c\psi_M^{\theta}(\theta) + \psi_{in}(c_i), \tag{1}$$

where the elastic energy is

$$\psi_{el} = 0.5\ \boldsymbol{\varepsilon_e} : \boldsymbol{E}(c_i) : \boldsymbol{\varepsilon_e}, \tag{2}$$

$\psi_0^{\theta}(\theta)$ and $\psi_M^{\theta}(\theta)$ are the thermal energy of austenite and martensite (the same for all martensitic variants), respectively, θ is the temperature, and $\psi_{in}(c_i)$ includes the energy of all interfaces and internal stress energy due to the lattice mismatch between austenite and martensitic variants. In the simplest case, it can be presented in the form

$$\psi_{in}(c_i) = Acc_0 + \sum_{i=1}^{m}\sum_{j=1}^{m} A_{ij}c_ic_j \geq 0\ ,\quad A > 0\ ,\quad A_{ij} \geq 0\ ,\quad A_{ii} = 0, \tag{3}$$

where A and A_{ij} are the coefficients. Schematic presentation of the non-convex free energy versus c for $A_{ij} = 0$ is given in Fig. 1a and b for a fixed elastic strain. Non-convexity of the energy is easy to obtain analytically. If we assume for simplicity that elastic moduli $\boldsymbol{E}$ is a linear function of c, then $\frac{\partial^2\psi}{\partial c^2} = -2A < 0$. Utilizing the second law of thermodynamics in the form of the Clausius–Planck inequality one can obtain the following expression for the dissipation rate

$$D = \sum_{i=1}^{m} X_{i0}\dot{c}_{i0} + \sum_{j=1}^{m-1}\sum_{i=j+1}^{m} X_{ij}\dot{c}_{ij} \geq 0. \tag{4}$$

The first term represents the dissipation rate due to the phase transformation from austenite to martensite and the second term is the dissipation rate for transformations between the martensite variants. The corresponding driving forces X_{i0} and X_{ij} are presented in Eqs. (10) and (11). The driving forces are positive for the phase transformations $0 \to i$ and $j \to i$ and negative for the opposite transformations.

Box 1 (Problem formulation). **Kinematics**

The additive total decomposition of the total strain, $\boldsymbol{\varepsilon}$, into elastic and transformational parts

$$\boldsymbol{\varepsilon} := \left(\frac{\partial \boldsymbol{u}}{\partial \boldsymbol{x}}\right)_s = \boldsymbol{\varepsilon}_e + \boldsymbol{\varepsilon}_t \tag{5}$$

Transformation strain $\boldsymbol{\varepsilon_t}$

$$\boldsymbol{\varepsilon_t} = \sum_{i=1}^{m} \boldsymbol{\varepsilon_{ti}} c_i \tag{6}$$

The volume fractions of phases and their rates

$$c = \sum_{i=1}^{m} c_i,\quad \sum_{i=0}^{m} c_i = c_0 + c = 1,\quad c_i \geq 0\quad \dot{c}_i = \sum_{j=0}^{m} \dot{c}_{ij},\quad \dot{c}_{ij} = -\dot{c}_{ji}, \tag{7}$$

Constitutive equations

Hooke's law:

$$\boldsymbol{\sigma} = \boldsymbol{E} : \boldsymbol{\varepsilon_e} \tag{8}$$

Tensor of elastic moduli

$$\boldsymbol{E} = \sum_{i=0}^{m} \boldsymbol{E}_i c_i \tag{9}$$

Thermodynamic driving forces for phase transformation from austenite to martensitic variant i

$$X_{i0} = \boldsymbol{\sigma} : \boldsymbol{\varepsilon_{ti}} - 0.5\ \boldsymbol{\varepsilon_e} : (\boldsymbol{E_i} - \boldsymbol{E_0}) : \boldsymbol{\varepsilon_e} - \left(\psi_M^{\theta} - \psi_0^{\theta}\right) - A(1-2c) - 2\sum_{k=1}^{m} A_{ik}c_k \geq 0,\quad i = 1, 2, \ldots, m;\ ,$$
$$A > 0\ ,\quad A_{ij} \geq 0\ ,\quad A_{ii} = 0 \tag{10}$$

Thermodynamic driving forces for transformation between marteniste variant j $\longrightarrow$ martensite variant i

$$X_{ij} = \boldsymbol{\sigma} : (\boldsymbol{\varepsilon_{ti}} - \boldsymbol{\varepsilon_{tj}}) - 0.5\ \boldsymbol{\varepsilon_e} : (\boldsymbol{E_i} - \boldsymbol{E_j}) : \boldsymbol{\varepsilon_e} - 2\sum_{k=1}^{m}(A_{ik} - A_{jk})c_k$$
$$j = 1, 2, \ldots, m-1,\quad i = j+1, j+2, \ldots, m \tag{11}$$

Phase transformation criterion:

Austenite $\longrightarrow$ i-th martensitic variant:

$$f_{i0}(\boldsymbol{\sigma}, c, \theta) = |X_{i0}| - k_{i0} \geq 0, i = 1, 2, \ldots, m;\quad k_{0j} = k_0 \forall j. \tag{12}$$

Martensitic variant j $\longrightarrow$ martensitic variant i

$$f_{ij}(\boldsymbol{\sigma}) = |X_{ij}| - k_{ij} \geq 0,\ j = 1, 2, \ldots, m-1,\quad i = j+1, j+2, \ldots, m \tag{13}$$

Evolution equations for the $\dot{c}_{ij}$:

$$f_{ij}(\boldsymbol{\sigma}, c, \theta) \geq 0 \implies \dot{c}_{ij} = \lambda_{ij}\mathrm{sign}(X_{ij})(|X_{ij}| - k_{ij}) \tag{14}$$

$$f_{ij}(\boldsymbol{\sigma}, c, \theta) < 0 \implies \dot{c}_{ij} = 0 \tag{15}$$
$$\text{where}\quad j = 0, 1, \ldots, m-1,\quad i = j+1, j+2, \ldots, m$$

$$\lambda_{ij} = \lambda_{ji},\qquad \lambda_{0j} = \lambda_0 \forall j. \tag{16}$$

$$\textit{Model A}:\ k_{i0} = 0;\quad \textit{Model B}:\quad k_{i0} \neq 0;\quad \textit{Model C}:\ k_{i0} = 0\quad \textit{for}\quad c_ic_0 \neq 0 \tag{17}$$

Equilibrium equations

$$\nabla \cdot \boldsymbol{\sigma} = 0 \tag{18}$$

Phase transformation criteria for phase transformations between austenite and martensitic variants and between martensitic variants are presented in Eqs. (12) and (13), respectively. Thus, transformation occurs when the magnitude of the driving force exceeds the corresponding athermal threshold k_{ij}. The athermal

Please cite this article as: S.E. Esfahani et al., Microscale phase field modeling of the martensitic transformation during cyclic loading of NiTi single crystal, International Journal of Solids and Structures (2018), https://doi.org/10.1016/j.ijsolstr.2018.03.022

threshold characterizes the resistance against a moving interface caused by the interactions between the interface and the long-range stress field of various defects (e.g., vacancies, dislocations, subgrain boundaries), by the Peierls barrier, acoustic emission, etc. Almost every micromechanical theory of the phase transformation incorporates such a term (Lim and McDowell, 2002; Levitas et al., 2010; Levitas and Ozsoy, 2009a; Boyd and Lagoudas, 1996a; Levitas et al., 1999; Gillet et al., 1998; Ozsoy and Babacan, 2016; Patoor and Berveiller, 1997). In contrast, the traditional phase field theories (Artemev et al., 2001; 2000; Levitas et al., 2010; Wang and Khachaturyan, 1997; Zhu et al., 2017; Cho et al., 2012; Idesman et al., 2008; Steinbach and Apel, 2006; Mosler et al., 2014; Schneider et al., 2015) neglect it, except (Levitas and Lee, 2007; Levitas et al., 2010).

We accept the linear kinetic Eqs. (14) and (15) for the rate of volume fraction $\dot{c}_{ij}$ and the net driving forces $|X_{ij}| - k_{ij}$, provided that the net driving forces are positive. This structure of equations is formally similar to the overstress viscoplastic models in the plasticity theory. The athermal thresholds and kinetic coefficients for the phase transformations between austenite and any of the martensitic variants are the same because the variants are connected by the symmetry operations of the cubic crystal structure. This fact leads to $k_{0i} = k_{0j} = k$ and $\lambda_{0i} = \lambda_{0j} = \lambda$. Martensitic variants can be divided into two groups: those that are in twin relationship with each other and those that are not. Within a group the variants have the same k_{ij} and λ_{ij} which are different between groups.

Three cases are considered in Eq. (17). For all these cases the threshold between martensitic variants is neglected, i.e., $k_{ij} = 0$ for all i, $j \neq 0$. Model A does not contain any athermal threshold. In this case the Onsager's reciprocal relations results in the symmetric kinetic coefficients, i.e., $\lambda_{ij} = \lambda_{ji}$. We will keep this symmetry for the models with athermal threshold as well. Model B utilizes constant thresholds k_{0j}. For this model, transformation may be arrested for some intermediate values of volume fractions, which may lead to an undesirable smeared microstructure. In light of this fact we use Model C with discontinuous athermal threshold. In this model the athermal threshold is nonzero prior to the initiation of phase transformation. As soon as the phase transformation criteria are satisfied no barrier for the phase transformation is considered, and states with intermediate values of volume fractions are not arrested. Thus, k_{0j} is considered as a nucleation threshold.

The equilibrium equation is accepted in traditional form of Eq. (18). The finite element algorithm used for solving the governing equations described in Box 1 is quite similar to that presented in Idesman et al. (2005).

Note that despite the non-uniqueness of the local equilibrium stress-strain curve in Fig. 1a, there is a uniqueness of the problem solution. The choice is performed with the help of the phase transformation criteria (12) and (13) and kinetic Eqs. (14) and (15) for the rate of volume fractions. The equilibrium stress-strain curve in Fig. 1a is not used for the solution of the problem, it is a result of the solution.

3. Problem formulation and material properties

The uniaxial loading of a rectangular NiTi plate (a commercially rolled nitinol with the nominal composition of Ni-49.75at.%Ti) (Kocich et al., 2011) is considered. The results are obtained for two-dimensional samples and by using 8-node biquadratic quadrilateral elements for all the simulations unless otherwise specified. The evolution of the martensitic microstructure in NiTi strips due to a cubic-monoclinic phase transformation is investigated under uniaxial cyclic loadings and plane strain conditions. Also, a discontinuous athermal threshold for the driving force (Model C) is considered in all the simulations where the athermal threshold is included. The temperature is assumed to be homogeneously distributed through the strip and it remains constant during the phase transformation. To avoid separation between martensitic variants and the necessity to track interfaces between them, we set $A_{ij} = 0$ for all i, $j \neq 0$. Then volume fraction of martensite c, which describes material instability, is the only order parameter. Volume fraction c_i for $i \neq 0$ do not describe material instabilities and are the traditional internal variables.

The transformation strain matrices associated with the twelve variants for the cubic-monoclinic phase transition are presented in Bhattacharyya (2003) and given below:

$$\varepsilon_{t1} = \begin{pmatrix} \gamma-1 & \beta & \beta \\ \beta & \alpha-1 & \delta \\ \beta & \delta & \alpha-1 \end{pmatrix} \quad \varepsilon_{t2} = \begin{pmatrix} \gamma-1 & -\beta & -\beta \\ -\beta & \alpha-1 & \delta \\ -\beta & \delta & \alpha-1 \end{pmatrix}$$

$$\varepsilon_{t3} = \begin{pmatrix} \gamma-1 & -\beta & \beta \\ -\beta & \alpha-1 & -\delta \\ \beta & -\delta & \alpha-1 \end{pmatrix}$$

$$\varepsilon_{t4} = \begin{pmatrix} \gamma-1 & \beta & -\beta \\ \beta & \alpha-1 & -\delta \\ -\beta & -\delta & \alpha-1 \end{pmatrix} \quad \varepsilon_{t5} = \begin{pmatrix} \alpha-1 & \beta & \delta \\ \beta & \gamma-1 & \beta \\ \delta & \beta & \alpha-1 \end{pmatrix}$$

$$\varepsilon_{t6} = \begin{pmatrix} \alpha-1 & -\beta & \delta \\ -\beta & \gamma-1 & -\beta \\ \delta & -\beta & \alpha-1 \end{pmatrix}$$

$$\varepsilon_{t7} = \begin{pmatrix} \alpha-1 & -\beta & -\delta \\ -\beta & \gamma-1 & \beta \\ -\delta & \beta & \alpha-1 \end{pmatrix} \quad \varepsilon_{t8} = \begin{pmatrix} \alpha-1 & \beta & -\delta \\ \beta & \gamma-1 & -\beta \\ -\delta & -\beta & \alpha-1 \end{pmatrix}$$

$$\varepsilon_{t9} = \begin{pmatrix} \alpha-1 & \delta & \beta \\ \delta & \alpha-1 & \beta \\ \beta & \beta & \gamma-1 \end{pmatrix}$$

$$\varepsilon_{t10} = \begin{pmatrix} \alpha-1 & \delta & -\beta \\ \delta & \alpha-1 & -\beta \\ -\beta & -\beta & \gamma-1 \end{pmatrix} \quad \varepsilon_{t11} = \begin{pmatrix} \alpha-1 & -\delta & \beta \\ -\delta & \alpha-1 & -\beta \\ \beta & -\beta & \gamma-1 \end{pmatrix}$$

$$\varepsilon_{t12} = \begin{pmatrix} \alpha-1 & -\delta & -\beta \\ -\delta & \alpha-1 & \beta \\ -\beta & \beta & \gamma-1 \end{pmatrix}, \tag{19}$$

where $\alpha = 1.0243$, $\beta = -0.0427$, $\gamma = 0.9563$, and $\delta = 0.058$ (Knowles and Smith, 1981; Hane and Shield, 1999). The material parameters used in the simulations are: $A = 13$ MPa, chosen to reproduce nucleation stresses for highly textured polycrystalline NiTi, used to determine properties of a single crystalline NiTi; $\lambda_{ij} = 10$ MPa ($j = 0, 1, \ldots, 11$, and $i = j+1, j+2, \ldots, 12$) to ensure that the rate of transformation is larger than the rate of straining; and $(\psi_i - \psi_0) = 18$ MPa (Gall et al., 2001; 1998). In contrast to polycrystalline aggregates, single crystal shape memory alloys exhibit elastic anisotropy in both martensite and austenite phases (Thomasová et al., 2017). The elastic constants for the austenite and one of the martensitic variants are presented in Eq. (20) (Thomasová et al., 2017):

$$[E_A] = \begin{bmatrix} 169 & 138 & 138 & 0 & 0 & 0 \\ 138 & 169 & 138 & 0 & 0 & 0 \\ 138 & 138 & 169 & 0 & 0 & 0 \\ 0 & 0 & 0 & 40 & 0 & 0 \\ 0 & 0 & 0 & 0 & 40 & 0 \\ 0 & 0 & 0 & 0 & 0 & 40 \end{bmatrix} (GPa),$$

$$[E_M] = \begin{bmatrix} 223 & 129 & 99 & 0 & 0 & 27 \\ 129 & 241 & 125 & 0 & 0 & -9 \\ 99 & 125 & 200 & 0 & 0 & 4 \\ 0 & 0 & 0 & 76 & -4 & 0 \\ 0 & 0 & 0 & -4 & 45 & 0 \\ 27 & -9 & 4 & 0 & 0 & 90 \end{bmatrix} (GPa). \tag{20}$$

The schematic view of a rectangular single crystal plate under a uniaxial cyclic loading and plane strain conditions, as well as the

Please cite this article as: S.E. Esfahani et al., Microscale phase field modeling of the martensitic transformation during cyclic loading of NiTi single crystal, International Journal of Solids and Structures (2018), https://doi.org/10.1016/j.ijsolstr.2018.03.022

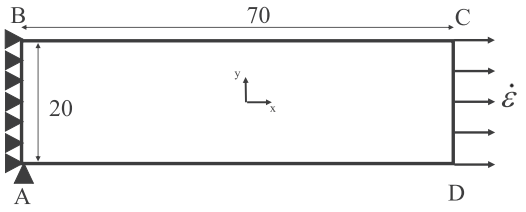

Fig. 2. A single crystalline rectangular plate under a uniaxial tensile loading and the corresponding boundary conditions.

corresponding boundary conditions are presented in Fig. 2. The implemented boundary conditions are: displacements $u_x = u_y = 0$ on the AB surface; normal σ and shear τ stresses $\sigma = \tau = 0$ along BC and AD surfaces (the free surfaces); and the lateral displacement $u_y = 0$ along with a constant velocity v_x, corresponding to the strain rate $\dot{\varepsilon}$ at the CD boundary. Initial values of volume fraction of martensitic variants c_j and both displacement fields in the sample are zero. When we mimic a heterogeneous nucleation site of martensite the volume fraction in one element is set as $c_i = 1$. Actual nucleation at strong pre-existing defects should be studied within nanoscale phase field models, e.g., Levitas and Javanbakht (2014), Javanbakht and Levitas (2016), and Wang and Li (2010). The orientation of the single crystal with respect to the coordinate axes of the sample is presented following Bunge Euler angle convention, where ϕ_1, ϕ, and ϕ_2 are three consecutive rotations along z-axis, x-axis, and the rotated z-axis (i.e., z'-axis). The results presented in this study are for (86°, 17°, 0°) and (0°, 0°, 0°) crystal orientations. The rotated transformation strains and elastic moduli can be calculated as follows

$$[\varepsilon_{ti}]^{\phi} = [R]^T[\varepsilon_{ti}][R] \tag{21}$$

$$[E]^{\phi} = [R]^T[R]^T[E][R][R]; \tag{22}$$

where $[\varepsilon_{ti}]$ and $[E]$ are given by Eqs. (19) and (20), respectively, and the rotation matrix is determined according to Eq. (23)

$$[R] = \begin{bmatrix} cos(\varphi_2) & \sin(\varphi_2) & 0 \\ -sin(\varphi_2) & \cos(\varphi_2) & 0 \\ 0 & 0 & 1 \end{bmatrix}\begin{bmatrix} 1 & 0 & 0 \\ 0 & \cos(\varphi) & \sin(\varphi) \\ 0 & -sin(\varphi) & \cos(\varphi) \end{bmatrix} \times \begin{bmatrix} cos(\varphi_1) & \sin(\varphi_1) & 0 \\ -sin(\varphi_1) & \cos(\varphi_1) & 0 \\ 0 & 0 & 1 \end{bmatrix}. \tag{23}$$

4. Numerical results and discussion

4.1. Study of mesh-sensitivity of solutions

It is known that for the constitutive equations which exhibit material instabilities due to strain softening the numerical solutions may be mesh sensitive in terms of both size and regularity of mesh. In the current paper mesh sensitivity studies are performed to ensure that the presented results are practically independent of the mesh density and its regularity. To this end several evaluations with various mesh densities as well as regular meshes with quadratic elements and irregular meshes with trapezoidal elements are presented in Figs. 3 and 4. The macrostrain rate and the crystal orientation are the same for the results presented in these two figures. For all the meshes the distributions of the volume fraction of austenite are very similar. The only difference is in the width of the transition zone between austenite and martensite, i.e., the finite-width (diffuse) interface. This is the only region where constitutive equations exhibit strain softening; for smaller local strains in the austenite region and for larger local strains in the martensitic bands, deformation behavior is stable. Since in the local stress-strain curve softening is followed by hardening in the martensitic region, the phase transformation within the martensitic bands and the width of the martensitic bands are practically mesh-independent for a fine enough mesh. The width of diffuse interfaces is stabilized and determined by the local strain rate. Due to this dependency the width of diffuse interfaces is sensitive to the macrostrain rate (or displacement rate) and mesh size (Ozsoy and Babacan, 2016; Nemat-Nasser and Choi, 2005; Nemat-

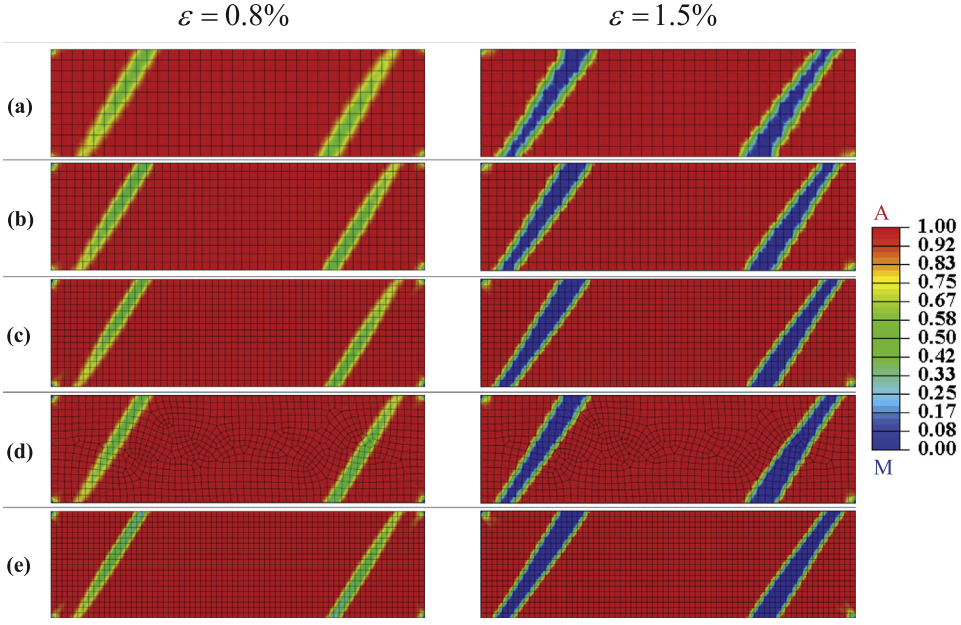

Fig. 3. The distributions of the volume fraction of austenite (c_0) with different FE meshes for $\dot{\varepsilon} = 5.5 \times 10^{-2}$ 1/s, prescribed uniaxial strains of $\varepsilon = 0.008$ and $\varepsilon = 0.015$, without athermal threshold and for the crystal orientation of $(\phi_1, \phi, \phi_2) = (86°, 17°, 0°)$. (a) 350, (b) 611, (c) 986, (d) 986 (unstructured) and (e) 1400 eight-node biquadratic elements.

Please cite this article as: S.E. Esfahani et al., Microscale phase field modeling of the martensitic transformation during cyclic loading of NiTi single crystal, International Journal of Solids and Structures (2018), https://doi.org/10.1016/j.ijsolstr.2018.03.022

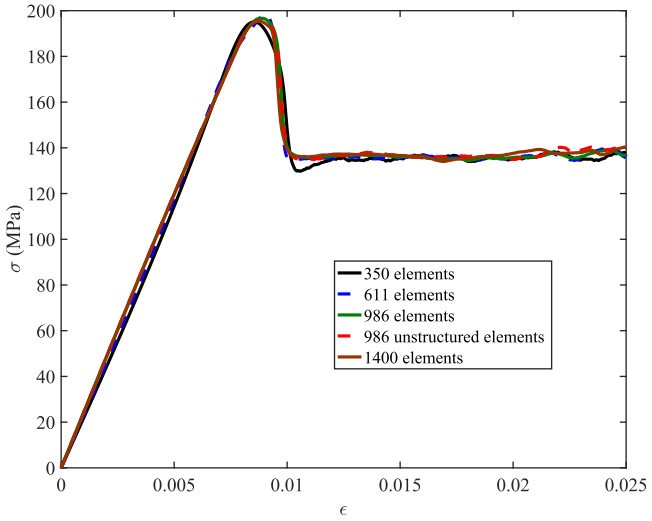

Fig. 4. The effect of various FE meshes on the global stress-strain curves for $\dot{\varepsilon} = 5.5 \times 10^{-2}\ 1/s$, without athermal threshold, and for Bunge Euler angle set (86°, 17°, 0°).

Nasser et al., 2005). While theoretically the problem is well posed and strain-rate regularized (similar to the viscoplastic regularization Beissel and Belytschko, 1996), when the loading or unloading rates approach zero to obtain a stationary solution the rate-dependency disappears and the stationary solution associates with a sharp interface between two adjacent phases. In numerical solutions the interface thickness is restricted to at least one finite element, as shown in Fig. 3, which leads to the mesh-size sensitivity of the interface width. This mesh-dependence of the stationary solution is unavoidable within local models with strain softening. Therefore, it is necessary to determine the contribution of mesh dependency to the results presented here.

In Fig. 4, the calculated global pseudo-elastic responses are presented. Small fluctuations are observed in the material response for different strains depending on the adopted meshes. However, this difference is quite small and not essential. Excluding the case with the smallest number of elements, 350, all the other four responses converge to practically the same solution. The only minor difference is observed for 350 FE in the region of the strong stress drop at the beginning of phase transformation. The broader the martensitic bands are the smaller the relative width of austenite-martensite interfaces is and the smaller the effect of meshes. The solution with the unstructured mesh does not differ essentially from that for the regular quadratic mesh. Thus, despite the unavoidable mesh-sensitivity of the width of the diffuse interface, the morphology of the transformed region and the global stress-strain curves are practically mesh-insensitive for fine enough mesh sizes. This is consistent with some previous studies (Idesman et al.,

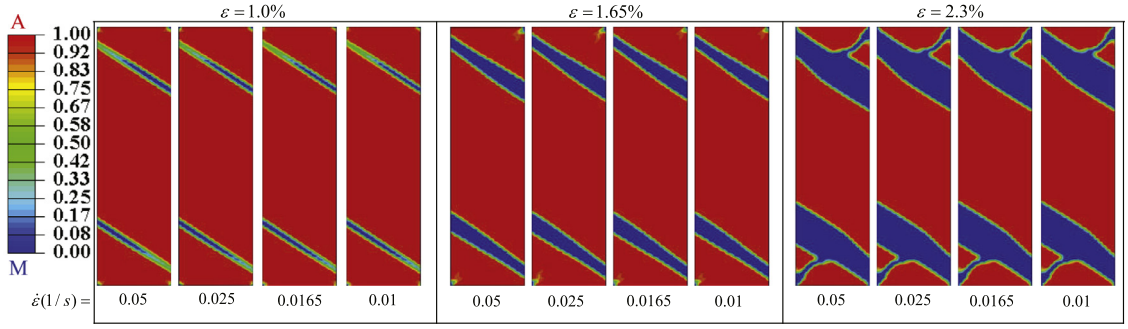

(a)

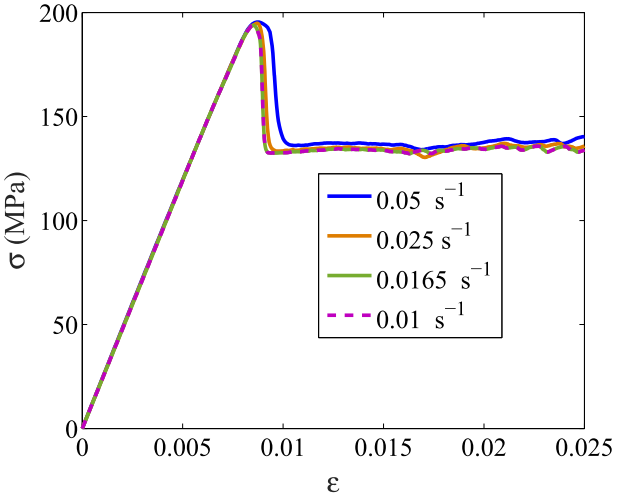

(b)

Fig. 5. The effects of strain rate for 981 biquadratic quadrilateral FE model without athermal threshold on (a) the distribution of the volume fraction of martensite at different macro-strains and (b) the corresponding stress-strain curves.

Please cite this article as: S.E. Esfahani et al., Microscale phase field modeling of the martensitic transformation during cyclic loading of NiTi single crystal, International Journal of Solids and Structures (2018), https://doi.org/10.1016/j.ijsolstr.2018.03.022

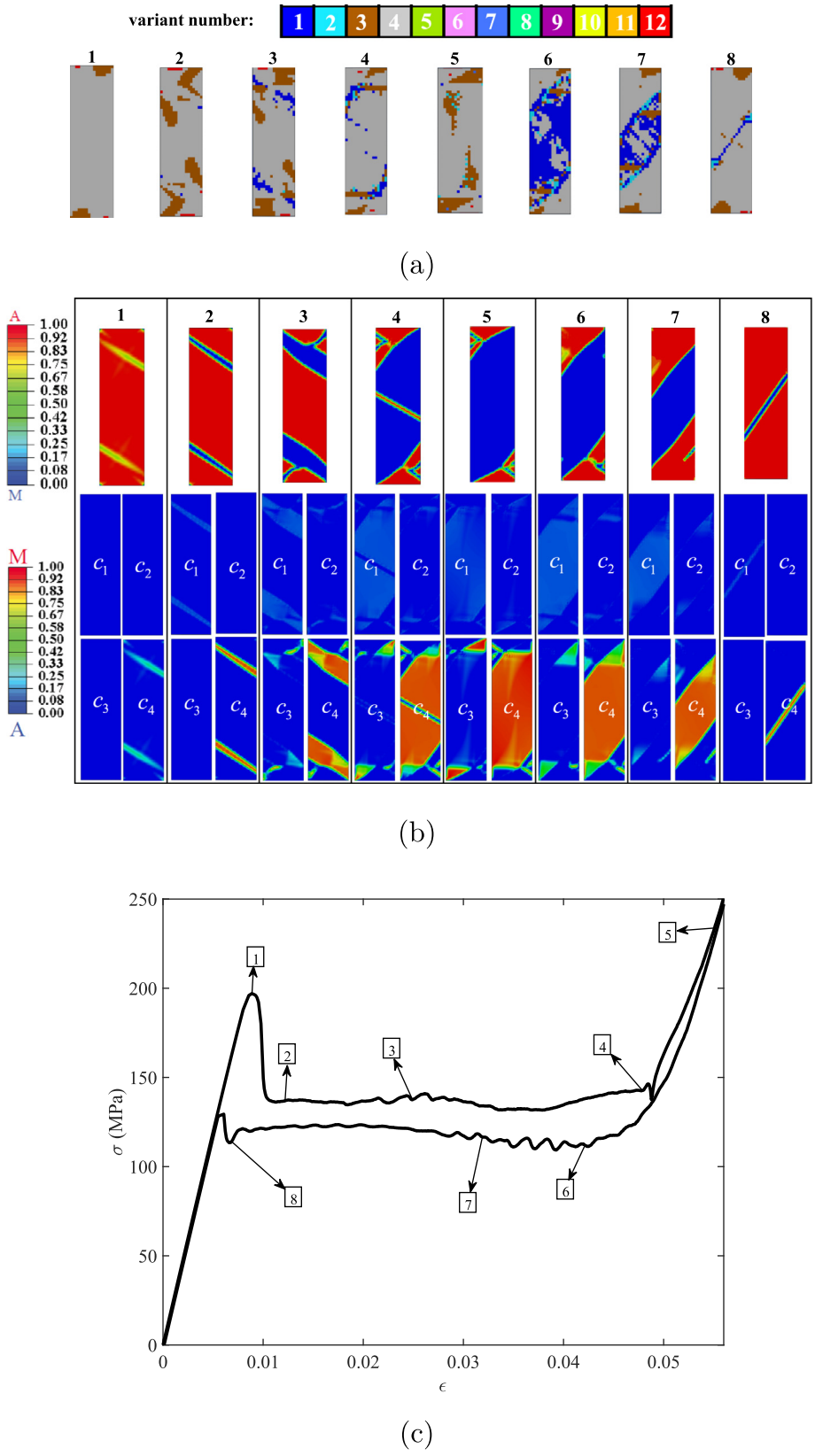

Fig. 6. Simulation results for a sample under a cyclic loading, without athermal threshold, for $\dot{\varepsilon} = 0.0165\ s^{-1}$, 981 eight-node biquadratic FE, and $(\phi_1, \phi, \phi_2) = (86^\circ, 17^\circ, 0^\circ)$. (a) The variant number for which the local mechanical part of the driving force based on local stresses is maximum; (b) the volume fraction of the martensite and martensitic variants, and (c) the stress-strain curve.

Please cite this article as: S.E. Esfahani et al., Microscale phase field modeling of the martensitic transformation during cyclic loading of NiTi single crystal, International Journal of Solids and Structures (2018), https://doi.org/10.1016/j.ijsolstr.2018.03.022

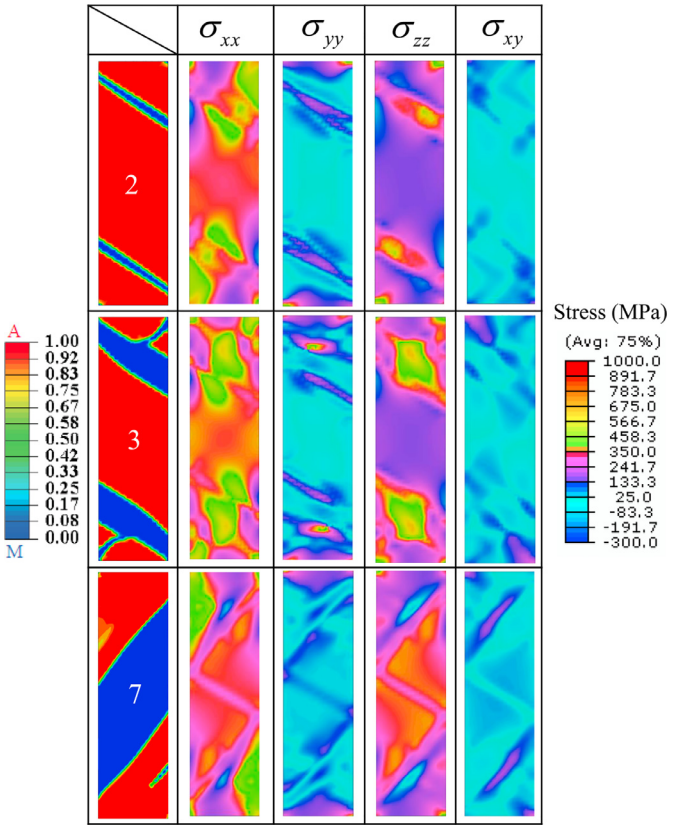

Fig. 7. The correlation between the microstructure evolution and the stress fields for three macrostrains presented in Fig. 6.

2005; Grossmann et al., 2010; Azadi et al., 2007). From here on, only the results for the 981-element model are presented.

Obtained practical mesh independence is in contrast to the results for models without a strain hardening part that follows after softening which are employed to model shear bands in elastoplastic materials (Beissel and Belytschko, 1996). For these models the entire shear band zone is unstable, and the width of the shear band is drastically mesh-size- and element-shape- sensitive.

4.2. Effect of the strain rate

The microstructure evolution in the sample and the stress-strain curves for four different strain rates are investigated. As shown in Fig. 5a, although the increase in strain rates indistinctly affects the interface widths and the morphology of the martensite bands near the sample ends, it changes the stress-strain curves for $\dot{\varepsilon} = 0.05\ s^{-1}$ only. This change is not strong and based on Fig. 5b, for smaller strain rates, all stress-strain curves overlap. Consequently, the obtained results can be considered a strain-rate insensitive for the strain rates smaller than $(0.0165 - 0.025)\ s^{-1}$. This is desirable because the effect of strain rate in the pseudoelastic behavior of shape memory alloys is usually related to the thermoelastic and transformation heating (Shaw and Kyriakides, 1997b), and strain rate dependence in the current model was mostly motivated by mathematical regularization of otherwise ill-posed problem formulation. Due to the formation of transformation-deformation bands the strain rate dependence of the local constitutive equations slightly changes the microstructure and the global stress-strain curves, especially for relatively small strain rates.

4.3. Cyclic loading

In Fig. 6b, the microstructure evolution in a single crystal sample loaded to different macrostrains is presented. For comparison, variant numbers for which the local transformation work is maximal are shown in Fig. 6a. It is clear that while in some regions this simplified criterion for the variant selection shows dominant variants, generally it does not fully reproduce the martensitic microstructure in 6 b, especially during unloading. This is because there is possibility of mixing variants with a reduction in the energy. For the chosen crystal orientation just four martensite variants are involved dominantly during the phase transformation and the volume fractions of the other variants are zero or negligible. The phase transformation produces the crystallographic variants which maximize the mechanical part of the driving force after their mixing. Between these four, variant 4 is more favorable in the major part of the sample and variant 3 is more favorable at regions close to the corners, relaxing bending stresses. The macroscopic uniaxial stress-strain curve in Fig. 6c demonstrates the generic properties identified by the localized phase transformation. In Fig. 7 one can see the stress fields for three different macrostrains. Interfaces do not perturb σ_{xx}, slightly perturb σ_{xy} and σ_{zz}, and are mostly visible in σ_{yy}, causing local stress concentration. The stress σ_{zz}, due to plane strain constraint, is comparable to σ_{xx}. Stresses σ_{yy} and σ_{xy} are much smaller excluding some stress concentrations.

Due to the effect of boundary conditions, in accordance with the experimental observations and calculations based on much simpler models (Shaw and Kyriakides, 1997a; Hallai and Kyriakides, 2013), the stress concentration locally triggers the initiation of phase transformation at the corners. However, since the volume fraction of the martensite, local and especially averaged over the sample, is very small, it does not have a considerable effect on the global stress-strain curve. In addition, due to the internal stresses that appear during phase transformation and bending (caused by the loss of geometric symmetry), the local stresses are not uniaxial anymore. All these facts lead to global stresses at point 1 that exceed the local uniaxial stress for austenite instability (Roytburd, 1993; Roytburd and Slutsker, 1997; 2001; Levitas and Ozsoy, 2009a; 2009b). Just after point 1 the stress-strain curve exhibits a noticeable drop after the onset of two martensite bands. This drop is ended by the completion of phase transformation within a major part of these bands. After point 2 the applied stress is almost constant, which is called a plateau stress. Martensite grows through the propagation of the interfaces. As it was discussed the decreasing (unstable) branch of the local stress-strain curve is localized merely within the diffuse interfaces. Due to their relatively small area the instability inside the interfaces has a minor effect on the global stress-strain data. Multiple small oscillations in the stress-strain curve (e.g., around points 3, 6, and 7) appear due to the formation of plates and bands in different regions as well as reverse phase transformation during loading (e.g., in the right lower corner of a sample near points 4 and 5). The coalescence of two large martensitic regions exhibits itself as a stress dip just after point 4. Similarly, the coalescence of two large austenitic regions leads to a stress rise during the strain decrease after point 8. During the loading process between points 4 and 5 a small amount of martensite adds despite a significant stress growth, and the residual austenite retains near the sample corners. The slope of the stress-strain curve increases to the value of the elastic modulus for the martensite-residual austenite mixture. During unloading the "elastic" curve for martensite-austenite mixture is slightly lower than during loading, which is possible due to continuing direct phase transformation in the corner regions. At some reduced stresses the reverse transformation starts leading to the lower plateau at the stress-strain curve. Due to resid-

Please cite this article as: S.E. Esfahani et al., Microscale phase field modeling of the martensitic transformation during cyclic loading of NiTi single crystal, International Journal of Solids and Structures (2018), https://doi.org/10.1016/j.ijsolstr.2018.03.022

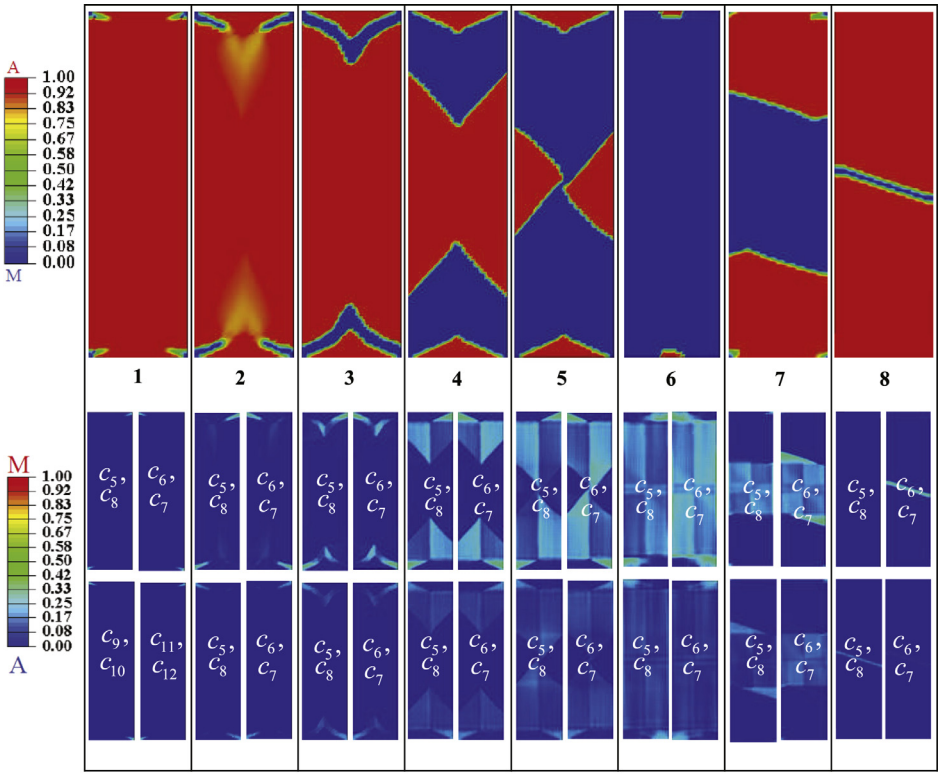

(a)

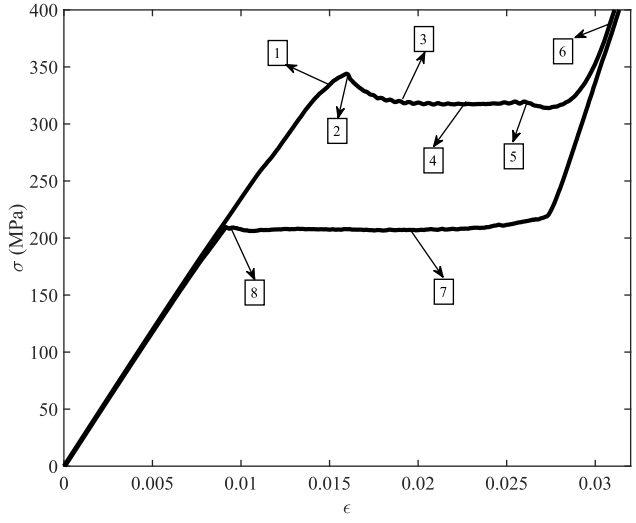

(b)

Fig. 8. (a) The microstructure evolution and (b) the stress-strain curve for a sample under a cyclic loading, for $\dot{\varepsilon} = 0.0165\, s^{-1}$, and $(\phi_1, \phi, \phi_2) = (0^\circ, 0^\circ, 0^\circ)$.

ual austenite and lack of necessity for nucleation of the austenite the stress-strain curve does not exhibit the stress peak between points 5 and 6, and the transition from "elastic" unloading to the reverse phase transformation plateau occurs smoothly. Although, while for a Model A with zero athermal threshold or Model C with a discontinuous athermal threshold the stress hysteresis is absent for the equilibrium phase transformation, a macroscopic stress hysteresis with the total dissipation of 1.145 MPa is observed in Fig. 6c. The corresponding dissipation is a viscous dissipation mostly within moving interfaces where strain rate is much larger than the prescribed one. Note that in the models without instabilities (Gillet et al., 1998; Thamburaja and Anand, 2001; Lim and McDowell, 2002; Govindjee and Miehe, 2001; Boyd and Lagoudas, 1996a; Levitas et al., 1998; 1999) the only way to explain stress hysteresis and dissipation (which form due to the phase transformation between austenite and martensite) is introducing athermal thresholds or distributed material heterogeneities.

4.4. Effect of crystal orientation

In experiments the onset of the martensitic phase transformation and the microstructure evolutions are strongly orientation-dependent (Acar et al., 2014; Karaca et al., 2012; 2013). It is note-

Please cite this article as: S.E. Esfahani et al., Microscale phase field modeling of the martensitic transformation during cyclic loading of NiTi single crystal, International Journal of Solids and Structures (2018), https://doi.org/10.1016/j.ijsolstr.2018.03.022

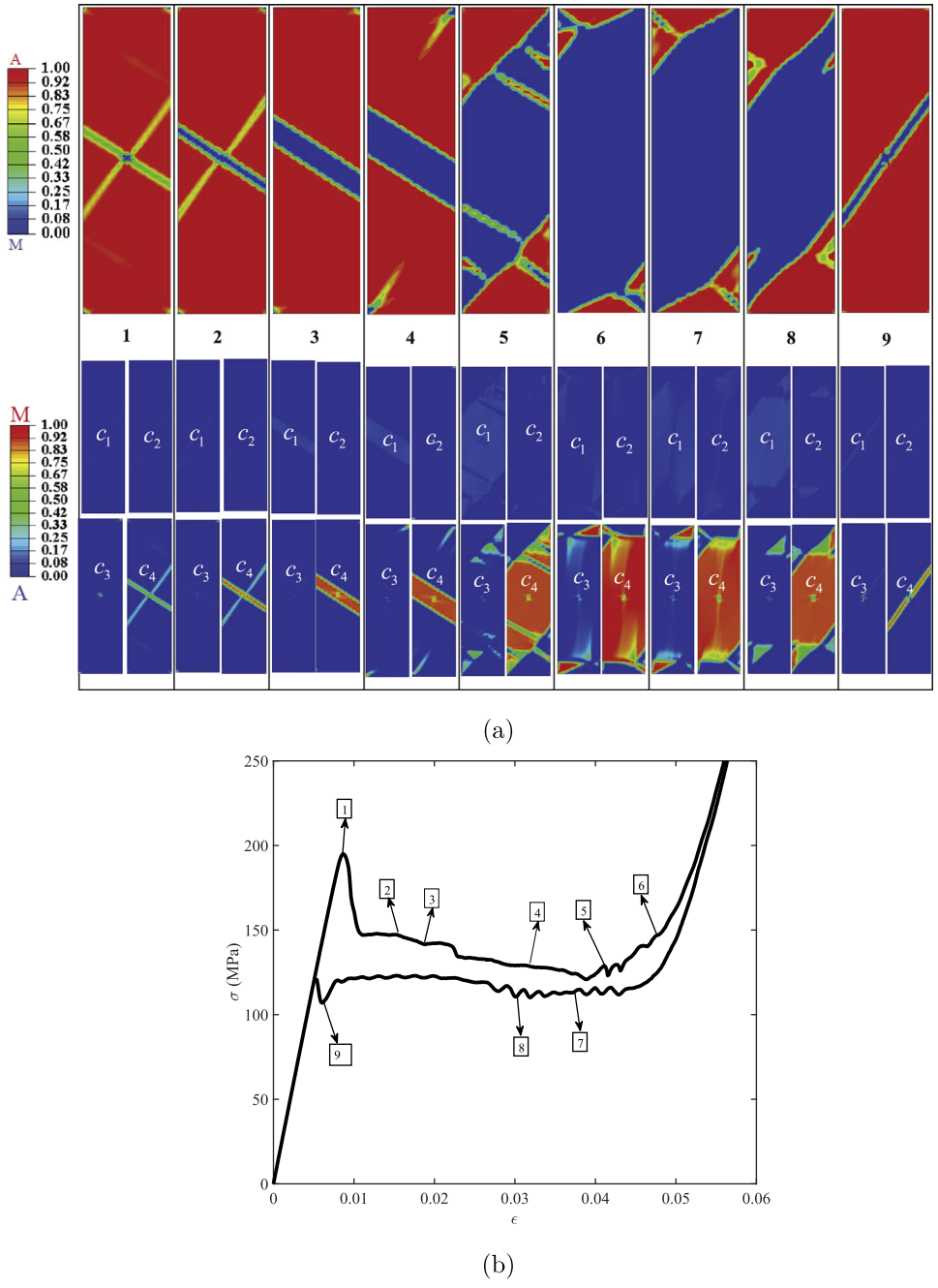

Fig. 9. (a) The microstructure evolution and (b) the stress-strain curve for a sample under a cyclic loading with a pre-existing nucleus in the middle, for $\dot{\varepsilon} = 0.0165\ s^{-1}$, and $(\phi_1, \phi, \phi_2) = (86^\circ, 17^\circ, 0^\circ)$.

worthy that the properties of a single crystal NiTi have been predicted by studying highly textured polycrystalline samples (Gall et al., 1998; 2001). However, since there are interactions and incompatibilities between grains, a parent phase grain never transforms completely to a product phase grain (Laplanche et al., 2017).

To investigate the influence of changing the crystal orientation with respect to the loading direction on the microstructure evolution and the macroscopic stress-strain response, a single crystal whose cubic axes coincide with the sample frame axes (i.e., $(\phi_1, \phi, \phi_2) = (0^\circ, 0^\circ, 0^\circ)$) is studied (see Fig. 8). Due to the symmetry of loading with respect to cubic lattice only eight variants with the tensile transformation strain in the loading direction, i.e. M_5 through M_{12}, appear. Some variants only differ by the signs of shears in the z direction. If they appear in the equal volume fractions, then transformation shears in the z direction will be absent which will reduce the internal stresses and their energy. Indeed, in simulations we found that $c_5 = c_8$, $c_6 = c_7$, $c_9 = c_{10}$, and $c_{11} = c_{12}$. In this case the stress concentrations around the corners are more favorable for the initiation of phase transformation in contrast to the previous examples with nonsymmetric orientation, in which phase transformation initiates near the bent locations. Since stress concentration decays away from the corners the initiation of the phase transformation is spread over a larger strain increment than for another orientation in Fig. 6b. This is the reason why the initiation first causes an increasing deviation from the linear elastic branch of austenite in Fig. 8b, then reaching the stress maximum followed by a smooth stress reduction to a plateau. The phase transformation starts at significantly higher stresses, and the to-

Please cite this article as: S.E. Esfahani et al., Microscale phase field modeling of the martensitic transformation during cyclic loading of NiTi single crystal, International Journal of Solids and Structures (2018), https://doi.org/10.1016/j.ijsolstr.2018.03.022

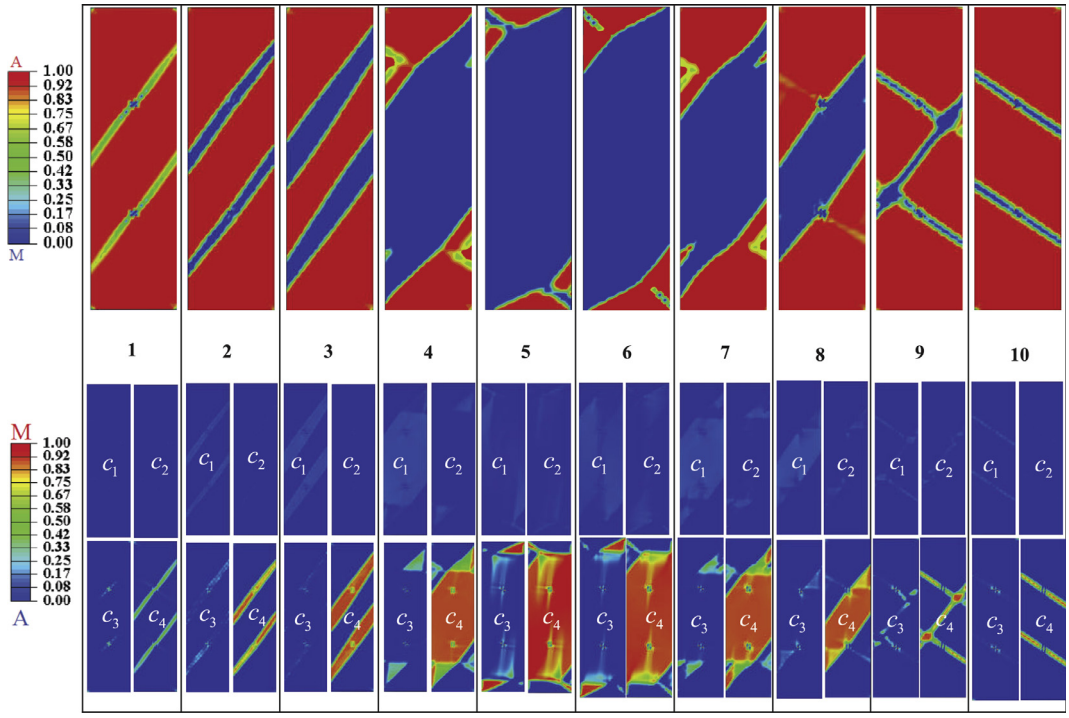

(a)

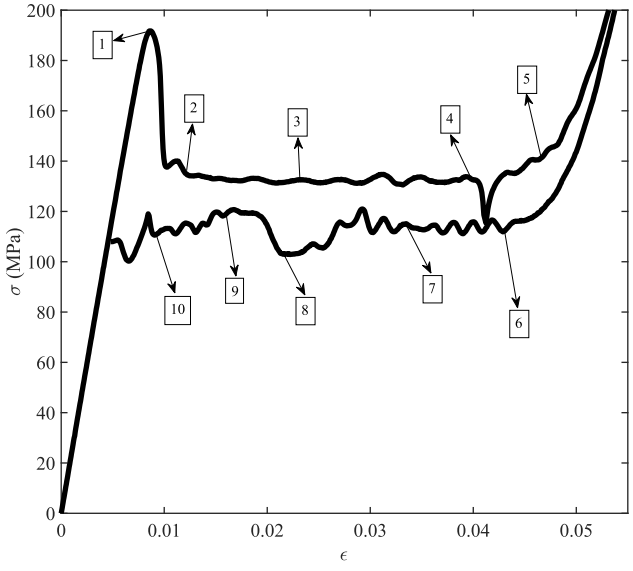

(b)

Fig. 10. (a) The microstructure evolution and (b) the stress-strain curve for a sample with two nuclei in the middle of a sample under a cyclic loading, for $\dot{\varepsilon} = 0.0165\ s^{-1}$, and $(\phi_1, \phi, \phi_2) = (86^\circ, 17^\circ, 0^\circ)$.

tal transformation strain (length of a plateau) is essentially smaller than the crystal orientation in Fig. 6b. The stress hysteresis is larger for the cubic orientation, and the total dissipation is 2.072 MPa which is approximately two times bigger than the case represented in Fig. 6.

A curvature in the microstructure of martensite observed in Fig. 8 is related to the variation of the relative contributions of different martensitic variants along the martensite band, mostly variants M_5, M_6, M_7, and M_8. This results in a variable averaged transformation strain which produces a variable invariant plane between the austenite and martensite mixture. At point 5 upper and lower martensite regions start their coalescence. Since this process is spread over some strain increment the stress reduction is small and the transition from the plateau segment to the elastic branch of martensite is smooth. The phase transformation in the sample is almost completed, but two small austenite regions near the symmetry plane of the sample provides smooth initiation of the reverse phase transformation during the unloading. The morphology of the martensite region during the reverse phase transformation is different than for the direct phase transformation: the martensite represents a single shrinking region with plane interfaces and small residual regions near the corners. The dependence

Please cite this article as: S.E. Esfahani et al., Microscale phase field modeling of the martensitic transformation during cyclic loading of NiTi single crystal, International Journal of Solids and Structures (2018), https://doi.org/10.1016/j.ijsolstr.2018.03.022

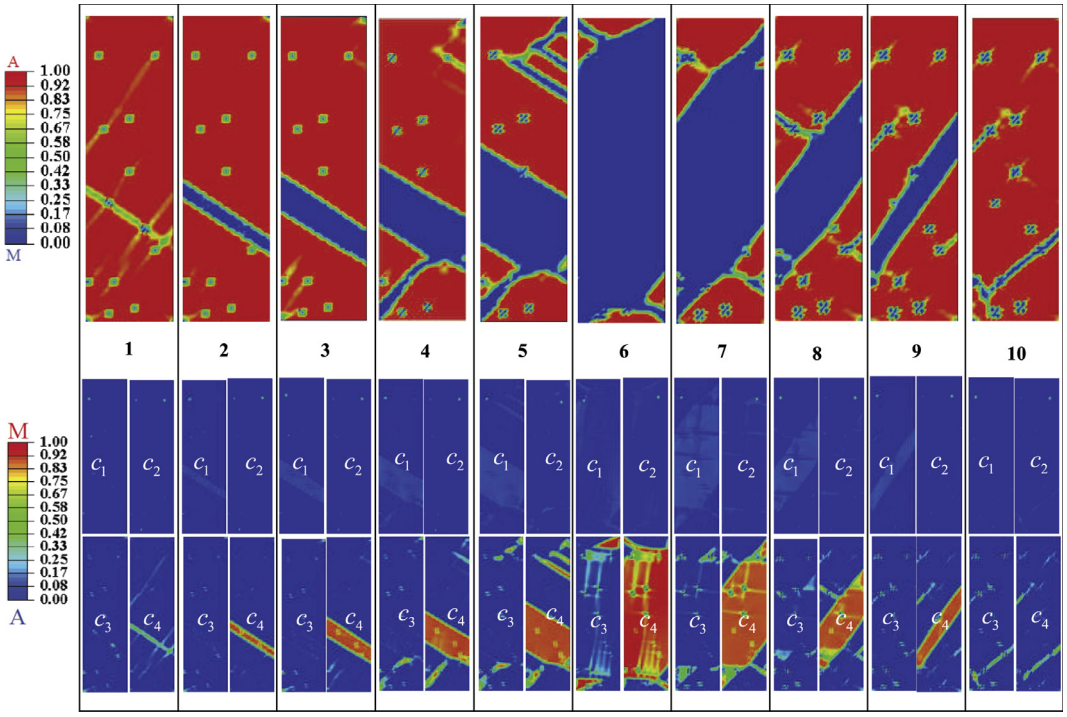

(a)

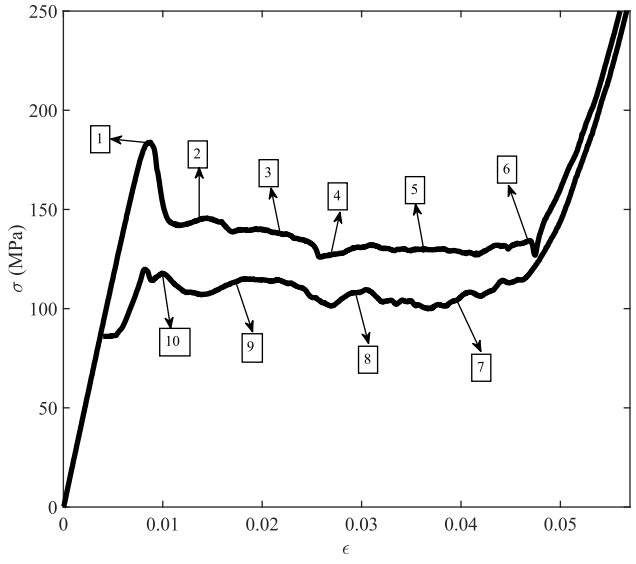

(b)

Fig. 11. (a) The microstructure evolution and (b) the stress-strain curve for a sample with twelve nuclei under a cyclic loading, for $\dot{\varepsilon} = 0.0165\ s^{-1}$, and $(\phi_1, \phi, \phi_2) = (86^\circ, 17^\circ, 0^\circ)$.

of the transformation stress and stress hysteresis on the crystal orientation is in qualitative agreement with both experimental (Gall et al., 2001; 1998) and numerical (Ozsoy and Babacan, 2016) results.

4.5. Effect of nucleation sites

The phase transformation is affected considerably by the pre-existing defects which serve as nucleation sites. To study the effect of defects on both microstructure evolution and macroscopic stress-strain relationship, specimens with one, two and twelve nuclei are treated as shown in Figs. 9, 10, and 11, respectively. For these examples all finite elements are initially austenite ($c = 0$) except those elements in which the volume fraction of a random martensite variant (as shown in the figures) is equal to one ($c_i = 1$). Phase transformation first initiates at these sites because the stress distribution around these nuclei produces a larger driving force for phase transformation than the other stress concentrators (e.g., corners). As shown in Fig. 9a-1, transforming regions appear initially in the form of two intersecting bands near the pre-existing nucleus. While the dominant band is expanding the orthogonal one is disappearing gradually due to the stress redistribution in the sample. This observation confirms that the reverse

Please cite this article as: S.E. Esfahani et al., Microscale phase field modeling of the martensitic transformation during cyclic loading of NiTi single crystal, International Journal of Solids and Structures (2018), https://doi.org/10.1016/j.ijsolstr.2018.03.022

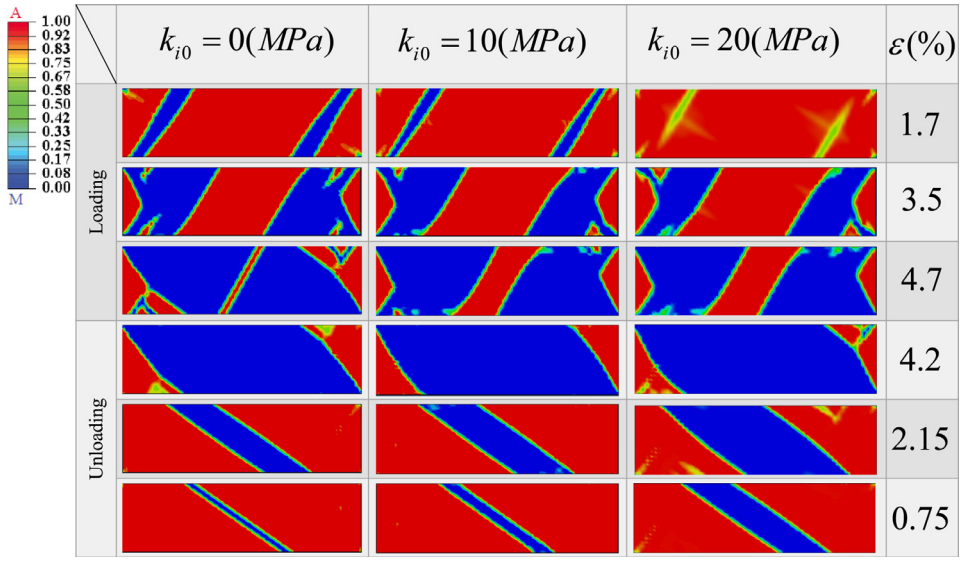

(a)

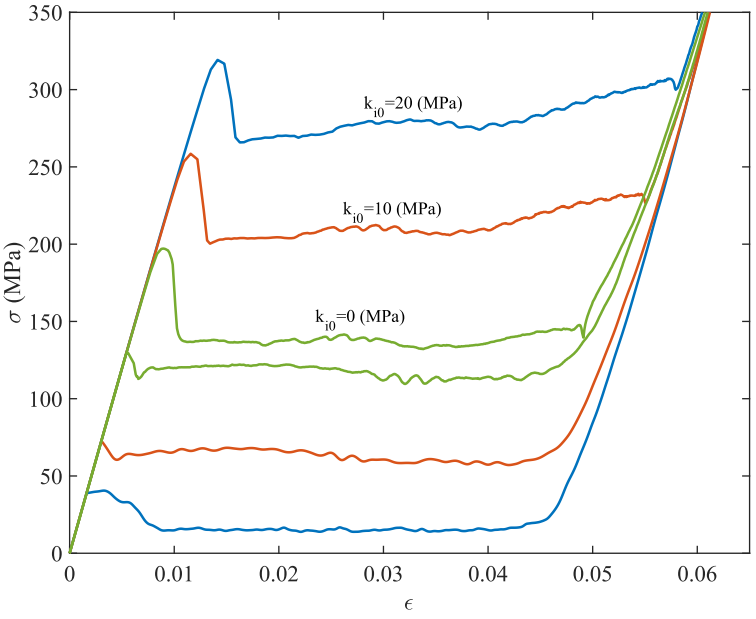

(b)

Fig. 12. (a) The effect of various athermal thresholds on the microstructure evolution and (b) the stress-strain curve for a sample under a cyclic loading, for $\dot{\varepsilon} = 0.0165\ s^{-1}$, and $(\phi_1, \phi, \phi_2) = (86^\circ, 17^\circ, 0^\circ)$.

phase transformation may happen under monotonic loading. The growth of the remaining band is accompanied by the appearance of two martensite regions at the two corners of the sample, as depicted in Fig. 9a-4. Moreover, as these two bands grow the stress distribution around them triggers the phase transformation near the bent locations at two free surfaces. All these interactions generate intersecting bands as shown in Fig. 9a-5. From points 3 to 5, during the formation of the intersecting bands, the corresponding macroscopic stress-strain diagram shows a negative slope because of an intense increase in the martensitic regions. The reverse phase transformation is practically unaffected by the pre-existing defect. The effects of two and twelve nucleating sites and their locations on the microstructure evolution during the loading-unloading process are presented in Figs. 10 and 11, respectively. Two nuclei in the middle of the sample participate in the initiation of the phase transformation. Subsequently, bending activates additional nuclei along with stress concentrators at the sample corners to form extra martensite bands. The reverse phase transformation is affected by nucleation sites at the very last stage of transformation during the disappearance of the last bands and retaining of small martensite regions near the nucleation sites. Interestingly, when the last martensite band in the middle of the sample disappears new martensite bands are activated by three nucleation sites (points 10 and 11).

When changing the number of nucleation sites and introducing all the variants as an the initial condition we obtained that only variants M_1, M_2, M_3, and M_4 are evolving during the phase transformation and other variants are not growing. Also, the increase in

Please cite this article as: S.E. Esfahani et al., Microscale phase field modeling of the martensitic transformation during cyclic loading of NiTi single crystal, International Journal of Solids and Structures (2018), https://doi.org/10.1016/j.ijsolstr.2018.03.022

the number of nucleation sites leads to a larger stress hysteresis. The stress hysteresis area (i.e., total dissipation) for the cases with no defect, one nucleation site, two nuclei, and twelve nuclei are 1.145 MPa, 1.3894 MPa, 1.4664 MPa, and 1.6101 MPa, respectively.

4.6. Effect of an athermal threshold

A model with discontinuous athermal threshold is utilized in which the threshold is introduced just for nucleation of the martensitic variant M_i or austenite, and it is drops to zero for any volume fraction of $0 < c_i < 0$. Without an athermal threshold the macroscopic stress-strain diagrams for all the previous examples had approximately the same total viscous dissipation, i.e., the hysteresis area. Comparison of the stress-strain curves along with the corresponding microstructure evolutions without and with two different athermal thresholds is presented in Fig. 12. In addition to the expected increase in the deviation of stresses from the equilibrium value for both direct and reverse phase transformations the stress for the direct martensitic phase transformation increases during the transformation (along with oscillations), while with no threshold it is practically constant. In contrast, during the reverse phase transformation the stress is almost constant for all cases. However, for $k_{i0} = 20$ MPa a significant rise of the stress occurs just before the completion of the reverse phase transformation. This result is observed because of delay in the disappearance of an intermediate band at the bottom left corner of the sample, see Fig. 12b for $\varepsilon = 0.75$ %. One can also see that increasing the athermal threshold postpones the initiation of the phase transformation in all the regions. Generally, for all cases the microstructure passes through very close configurations, but with some delay with increasing k_{i0}. As expected, the athermal threshold increases the stress hysteresis: hysteresis area is equal to 1.145 MPa, 7.203 MPa, and 12.476 MPa for cases with zero, 10 MPa and 20 MPa of the athermal threshold, respectively.

5. Concluding remarks

A constitutive model developed in Levitas et al. (2004) and Idesman et al. (2005) is slightly advanced and employed for studying the stress-induced cubic-monoclinic phase transition in NiTi single crystal. All 12 crystallographic variants of the martensite are included. This microscale phase field model tracks finite-width interfaces between austenite and the mixture of martensitic variants only and does not reproduce variant-variant interfaces. The model is scale-independent without the gradient term; the interface energy is implemented in the Helmholtz free energy in an average sense. Formal strain rate regularization of the problem is used which introduces some scale which, however, tends to zero for quasi-static loading. The model is implemented in FE ABAQUS code through a corresponding UMAT subroutine. Multiple problems for a uniaxial cyclic loading are solved to study the effect of different parameters on the stress-strain responses and microstructure evolution. Although stress hysteresis is absent in the local stress-strain response the global responses of the NiTi sample under the uniaxial loading exhibit hysteresis and corresponding dissipation in the macroscopic stress-strain curves due to the instability of the homogeneous deformations and large local strain rate within the finite-width interfaces. Obtained results show that solutions are practically mesh-independent in terms of both microstructure and global stress-strain curves, and are independent of the strain rate for relatively small strain rates. Introducing the defects in the sample leads to a decrease in the nucleation stress and more oscillations in the global stress-strain response, but increases total energy dissipation. The sudden drop in the stress-strain curve after initiation of the martensitic phase transformation due to the strain softening and localization in the sample and absence of a similar jump for the reverse transformation is in qualitative agreement with experimental results in the literature. Band-like microstructures obtained in simulations are observed in experiments as well. For different crystallographic orientations of a sample the variants which appear during the phase transformation, the geometry of a microstructure, the macroscopic stress-strain response, and the hysteresis loops are essentially different. Athermal threshold, in addition to the expected broadening of the hysteresis loop, leads to some strain hardening for the direct transformation but practically to the horizontal plateau (with some oscillations) for the reverse transformation.

The main advantages of the model (Levitas et al., 2004; Idesman et al., 2005) utilized here in comparison with traditional phase field models (Artemev et al., 2001; 2000; Levitas et al., 2010; Wang and Khachaturyan, 1997; Zhu et al., 2017; Cho et al., 2012; Idesman et al., 2008; Levin et al., 2013; Levitas, 2013; Levitas and Javanbakht, 2010; Levitas, 2014) are:

(a) since it is scale-free, much larger specimens can be treated numerically;
(b) interfaces between austenite and martensitic mixture are resolved only, without resolving variant-variant interfaces (which would require few nm scale resolution);
(c) athermal threshold for interface propagation and stress hysteresis can be included much easier than for traditional models, for which special approaches presented in Levitas and Lee (2007) and Levitas et al. (2010) should be applied.

The main advantage of the model (Levitas et al., 2004; Idesman et al., 2005) utilized here in comparison with phenomenological (Arghavani et al., 2010; Lexcellent et al., 2000; Panico and Brinson, 2007; Lagoudas et al., 2012; Zaki and Moumni, 2007) and micromechanical (Bo and Lagoudas, 1999; Saleeb et al., 2011) models is that it reproduces a discrete martensite-austenite microstructure. This allows one to better reproduce internal stresses and effective properties, which strongly depend on morphology of the multiphase mixture. In addition, micromechanical models, which take into account multiple martensitic variants (Bo and Lagoudas, 1999; Saleeb et al., 2011), operate with the habit plane variants instead of the Bain strain tensor. Bain-strain based approach is more strict because the transformation strain for the habit plane variants depends on stresses (Roytburd, 1993; Levitas and Ozsoy, 2009a; 2009b), which is neglected in the micromechanical models. Also, number of the Bain strain variants is much smaller than the number of the habit plane variants, e.g., 12 versus 192 for cubic to monoclinic transformation (Bhattacharyya, 2003).

Note that practically any previous phenomenological (Arghavani et al., 2010; Lexcellent et al., 2000; Panico and Brinson, 2007; Lagoudas et al., 2012; Zaki and Moumni, 2007) and micromechanical (Bo and Lagoudas, 1999; Saleeb et al., 2011) models can be easily transformed to a microscale phase field model and will reproduce discrete microstructure if one substitutes strain hardening with softening and the habit plane variants with the Bain strain variants. The above comparison was performed in Levitas et al. (2004) and Idesman et al. (2005) as well.

One of the terminological questions is whether the term "microscale phase field" introduced in Idesman et al. (2005) is appropriate for the current model? There is no strict answer to this question because there is no strict definition of what a "phase field" model is, and different communities and researchers use different meanings, which were not strictly formulated. From one side, if one considers, as a starting point, phenomenological or micromechanical models (Arghavani et al., 2010; Lexcellent et al., 2000; Panico and Brinson, 2007; Lagoudas et al., 2012; Zaki and Moumni, 2007; Bo and Lagoudas, 1999; Saleeb et al., 2011) (which are definitely not phase field models) and substitutes strain

Please cite this article as: S.E. Esfahani et al., Microscale phase field modeling of the martensitic transformation during cyclic loading of NiTi single crystal, International Journal of Solids and Structures (2018), https://doi.org/10.1016/j.ijsolstr.2018.03.022

hardening with softening to obtain a counterpart of a model in Levitas et al. (2004) and Idesman et al. (2005) and reproduces discrete microstructure, will this transform them to phase field models? The answer is not straightforward. It is more constructive to compare the model (Levitas et al., 2004; Idesman et al., 2005) with other phase field models. Like any phase field model, the model (Levitas et al., 2004; Idesman et al., 2005) utilized here is based on an order parameter, i.e., an internal variable that is responsible for material instability, which leads to localization of the order parameter and consequently transformation strain that reproduces discrete martensitic microstructure. Similar, like any phase field model, the model (Levitas et al., 2004; Idesman et al., 2005) utilized here includes nonconvex energy in terms of the order parameter. The volume fractions of phases as order parameters were used in the phase field literature (Steinbach and Apel, 2006; Tůma and Stupkiewicz, 2016; Mosler et al., 2014; Schneider et al., 2015). The only difference with the traditional phase field approach is that we neglected the gradient energy term. However, this is not unusual. Historically (Landau, 1965; Umantsev, 2012), the first phase field theory for phase transformations, namely Landau theory, did not contain a gradient energy as well. Only 13 years later, the gradient term was introduced by Ginzburg and Landau, and since then this theory is named after them. The gradient term was omitted in the phase field reaction-pathway approach to phase transformations (Denoual et al., 2010), dislocation evolution (Koslowski et al., 2002; Koslowski and Ortiz, 2004), phase field microelasticity theory for modeling structurally inhomogeneities like voids, cracks, and polycrystalline aggregates (Wang et al., 2002), elastoplastic phase field model (Guo et al., 2005), and phase field model for cavitation in liquid (Levitas et al., 2011). The gradient term was claimed to be insignificant for the phase field approach to crack propagation (Jin et al., 2001). Note that approaches in Wang et al. (2002) and Guo et al. (2005) even do not include instability and microstructure formation, which demonstrates that the term “phase field” is used in a very broad sense. Thus, there are no reasons that prevent naming this model a phase field model. The addition “microscale” distinguishes our model from the traditional nanoscale phase field models, similar to the additions “microelasticity” and “elastoplastic” in Wang et al. (2002) and Guo et al. (2005). Note that when the microscale and traditional nanoscale (Levitas and Javanbakht, 2014; Javanbakht and Levitas, 2016) phase field models are applied to similar problems, like those considered here with a single order parameter, or nucleation of martensite at the dislocation pileup (Levitas and Javanbakht, 2014; Javanbakht and Levitas, 2016), solutions with both models are very close.

This work represents a building block for investigations of the pseudoelastic properties of NiTi polycrystalline alloys which will be presented in the following paper.

Acknowledgments

VIL and SEE gratefully acknowledge the support of NSF (CMMI-1536925 and DMR-1434613), ARO (W911NF-17-1-0225) and the Iowa State University (Vance Coffman Faculty Chair Professorship). The simulations were performed at Extreme Science and Engineering Discovery Environment (XSEDE), allocations TG-MSS140033 and MSS170015. PCC and IG gratefully acknowledge the Center for Advanced Non-Ferrous Structural Alloys, which is a joint industry-university center between the Colorado School of Mines and the Iowa State University (NSF award 1624748).

References

Acar, E., Karaca, H.E., Tobe, H., Noebe, R.D., Chumlyakov, Y.I., 2014. Orientation dependence of the shape memory properties in aged ni 45.3 ti 29.7 hf 20 pd 5 single crystals. Intermetallics 54, 60–68.

Arghavani, J., Auricchio, F., Naghdabadi, R., Reali, A., Sohrabpour, S., 2010. A 3-d phenomenological constitutive model for shape memory alloys under multiaxial loadings. Int. J. Plast. 26, 976–991.

Artemev, A., Jin, Y., Khachaturyan, A.G., 2001. Three-dimensional phase field model of proper martensitic transformation. Acta Mater. 49, 1165–1177.

Artemev, A., Wang, Y., Khachaturyan, A.G., 2000. Three-dimensional phase field model and simulation of martensitic transformation in multilayer systems under applied stresses. Acta Mater. 48, 2503–2518.

Azadi, B., Rajapakse, R.K.N.D., Maijer, D.M., 2007. Multi-dimensional constitutive modeling of SMA during unstable pseudoelastic behavior. Int. J. Solids Struct. 44, 6473–6490.

Barsch, G.R., Krumhansl, J.A., 1984. Twin boundaries in ferroelastic media without interface dislocations. Phys. Rev. Lett. 53, 1069.

Beissel, S., Belytschko, T., 1996. On patterns of deformation in phase transformations and luders bands. Int. J. Solids Struct. 33, 1689–1707.

Bhattacharyya, K., 2003. Microstructure of martensite: Why it forms and how it gives rise to the shape-memory effect. Oxford Series on Materials Modelling, OUP Oxford.

Bo, Z., Lagoudas, D.C., 1999. Thermomechanical modeling of polycrystalline SMAs under cyclic loading, Part i: Theoretical derivations. Int. J. Eng. Sci. 37, 1089–1140.

Boyd, J.G., Lagoudas, D.C., 1996a. Thermodynamical constitutive model for shape memory materials, part i. Int. J. Plast. 12, 805–842.

Chang, B.C., Shaw, J.A., Iadicola, M.A., 2006. Thermodynamics of shape memory alloy wire: modeling, experiments, and application. Continuum. Mech. Thermodyn. 18, 83–118.

Cho, J.Y., Idesman, A.V., Levitas, V.I., Park, T., 2012. Finite element simulations of dynamics of multivariant martensitic phase transitions based on ginzburg-landau theory. Int. J. Solids Struct. 49, 1973–1992.

Churchill, C.B., Shaw, J.A., Iadicola, M.A., 2009. Tips and tricks for characterizing shape memory alloy wire: part 3-localization and propagation phenomena. Exp. Tech. 33, 70–78.

Denoual, C., Caucci, A.M., Soulard, L., Pellegrini, Y.P., 2010. Phase-field reaction-pathway kinetics of martensitic transformations in a model fe3ni alloy. Phys. Rev. Lett. 105, 035703.

Falk, F., 1983. Ginzburg-landau theory of static domain walls in shape-memory alloys. Z. Physik. B - Condensed Matter. 51, 177–185.

Gall, K., Sehitoglu, H., Anderson, R., Karaman, I., Chumlyakov, Y.I., Kireeva, I.V., 2001. On the mechanical behavior of single crystal niti shape memory alloys and related polycrystalline phenomenon. Mater. Sci. Eng. A. 317, 85–92.

Gall, K., Sehitoglu, H., Chumlyakov, Y.I., Zuev, Y.L., Karaman, I., 1998. The role of coherent precipitates in martensitic transformations in single crystal and polycrystalline ti-50.8 at%; ni. Scr. Mater. 39, 699–705.

Gillet, Y., Patoor, E., Berveiller, M., 1998. Calculation of pseudoelastic elements using a non-symmetrical thermomechanical transformation criterion and associated rule. J. Intell. Mater. Syst. Struct. 9, 366–378.

Govindjee, S., Miehe, C., 2001. A multi-variant martensitic phase transformation model: formulation and numerical implementation. Comput. Methods Appl. Mech. Eng. 191, 215–238.

Grossmann, C., Schaefer, A., Wagner, M.F.X., 2010. A finite element study on localized deformation and functional fatigue in pseudoelastic niti strips. Mater. Sci. Eng. A. 527, 1172–1178.

Guo, X.H., Shi, S.Q., Ma, X.Q., 2005. Elastoplastic phase field model for microstructure evolution. Appl. Phys. Lett. 87, 221910.

Hallai, J.F., Kyriakides, S., 2013. Underlying material response for Lüders-like instabilities. Int. J. Plast. 47, 1–12.

Hane, K.F., Shield, T.W., 1999. Microstructure in the cubic to monoclinic transition in titanium-nickel shape memory alloys. Acta Mater. 47, 2603–2617.

He, Y., Yin, H., Zhou, R., Sun, Q., 2010. Ambient effect on damping peak of NiTi shape memory alloy. Mater. Lett. 64, 1483–1486.

He, Y.J., Sun, Q.P., 2010. Macroscopic equilibrium domain structure and geometric compatibility in elastic phase transition of thin plates. Int. J. Mech. Sci. 52. 1198–211

Iadicola, M.A., Shaw, J.A., 2004. Rate and thermal sensitivities of unstable transformation behavior in a shape memory alloy. Int. J. Plast. 20, 577–605.

Idesman, A.V., Cho, J.Y., Levitas, V.I., 2008. Finite element modeling of dynamics of martensitic phase transitions. Appl. Phys. Lett. 93, 043102.

Idesman, A.V., Levitas, V.I., Preston, D.L., Cho, J.Y., 2005. Finite element simulations of martensitic phase transitions and microstructures based on a strain softening model. J. Mech. Phys. Solids. 53, 495–523.

Jacobs, A.E., 1992. Finite-strain solitons of a ferroelastic transformation in two dimensions. Phys. Rev. B. 46, 8080–8088.

Javanbakht, M., Levitas, V.I., 2016. Phase field simulations of plastic strain-induced phase transformations under high pressure and large shear. Phys. Rev. B. 94, 214104.

Jiang, D., Kyriakides, S., Bechle, N.J., Landis, C.M., 2017a. Bending of pseudoelastic NiTi tubes. Int. J. Solids Struct. 124, 192–214.

Jiang, D., Kyriakides, S., Landis, C.M., 2017b. Propagation of phase transformation fronts in pseudoelastic NiTi tubes under uniaxial tension. Extreme Mech. Lett. 15, 113–121.

Jiang, D., Kyriakides, S., Landis, C.M., Kazinakis, K., 2017. Modeling of propagation of phase transformation fronts in niti under uniaxial tension. Eur. J. Mech. A-Solids. 64, 131–142.

Jiang, D., Landis, C.M., Kyriakides, S., 2016. Effects of tension/compression asymmetry on the buckling and recovery of niti tubes under axial compression. Int. J. Solids Struct. 100, 41–53.

Jin, Y.M., Wang, Y.U., Khachaturyan, A.G., 2001. Three-dimensional phase field microelasticity theory and modeling of multiple cracks and voids. Appl. Phys. Lett. 79, 3071.
Karaca, H.E., Acar, E., Basaran, B., Noebe, R.D., Bigelow, G., Garg, A., Yang, F., Mills, M.J., Chumlyakov, Y.I., 2012. Effects of aging on [111] oriented nitihfpd single crystals under compression. Scr. Mater. 67, 728–731.
Karaca, H.E., Acar, E., Ded, G.S., Basaran, B., Tobe, H., Noebe, R.D., Bigelow, G., Chumlyakov, Y.I., 2013. Shape memory behavior of high strength nitihfpd polycrystalline alloys. Acta Mater. 61, 5036–5049.
Knowles, K.M., Smith, D.A., 1981. The crystallography of the martensitic transformation in equiatomic Nickel-Titanium. Acta Metall. 29, 101–110.
Kocich, R., Kursa, M., Szurman, I., 2011. The influence of imposed strain on the development of microstructure and transformation characteristics of ni-ti shape memory alloys. J. Alloys Compd. 509, 2716–2722.
Koslowski, M., Cuitino, A., Ortiz, M., 2002. A phase-field theory of dislocations dynamics, strain hardening and hysteresis in ductile single crystals. J. Mech. Phys. Solids. 50, 2597–2635.
Koslowski, M.A., Ortiz, M., 2004. A multi-phase field model of planar dislocation networks. Model. Simul. Mater. Sci. Eng. 12, 1087–1097.
Lagoudas, D., Hartl, D., Chemisky, Y., Machado, L., Popov, P., 2012. Constitutive model for the numerical analysis of phase transformation in polycrystalline shape memory alloys. Int. J. Plast. 32, 155–183.
Lagoudas, D.C., 2008. Shape memory alloys. Science and Business Media. LLC.
Landau, L.D., 1965. Collected papers of l. d. landau. Gordon and Breach, NewYork.
Laplanche, G., Birk, T., Schneider, S., Frenzel, J., Eggeler, G., 2017. Effect of temperature and texture on the reorientation of martensite variants in niti shape memory alloys. Acta Mater. 127, 143–152.
Levin, V.A., Levitas, V.I., Zingerman, K.M., Freiman, E.I., 2013. Phase-field simulation of stress-induced martensitic phase transformations at large strains. Int. J. Solids Struct. 50, 2914–2928.
Levitas, V.I., 2013. Phase-field theory for martensitic phase transformations at large strains. Int. J. Plast. 49, 85–118.
Levitas, V.I., 2014. Phase field approach to martensitic phase transformations with large strains and interface stresses. J. Mech. Phys. Solids 70, 154–189.
Levitas, V.I., Idesman, A.V., Palakala, A., 2011. Phase-field modeling of fracture in liquid. J. Applied Physics 110, 033531.
Levitas, V.I., Idesman, A.V., Preston, D.L., 2004. Microscale simulation of martensitic microstructure evolution. Phys. Rev. Lett. 93, 105701.
Levitas, V.I., Idesman, A.V., Stein, E., 1999. Shape memory alloys: micromechanical modelingand numerical analysis of structures. J. Intell. Mater. Syst. Struct. 10, 983–996.
Levitas, V.I., Idesman, A.V., Stein, E., Spielfeld, J., Hornbogen, E., 1998. Simple micromechanical model for pseudoelastic behavior of cuznal alloy. J. Intell. Mater. Syst. Struct. 9, 324–334.
Levitas, V.I., Javanbakht, M., 2010. Surface tension and energy in multivariant martensitic transformations: phase-field theory, simulations, and model of coherent interface. Phys. Rev. Lett. 105, 165701.
Levitas, V.I., Javanbakht, M., 2011. Surface-induced phase transformations: multiple scale and mechanics effects and morphological transitions. Phys. Rev. Lett. 107 (17), 175701.
Levitas, V.I., Javanbakht, M., 2014. Phase transformations in nanograin materials under high pressure and plastic shear: nanoscale mechanisms. Nanoscale 6, 162–166.
Levitas, V.I., Lee, D.W., 2007. Athermal resistance to interface motion in the phase–field theory of microstructure evolution. Phys. Rev. Lett. 99, 245701.
Levitas, V.I., Lee, D.W., Preston, D.L., 2010. Interface propagation and microstructure evolution in phase field models of stress-induced martensitic phase transformations. Int. J. Plast. 26, 395–422.
Levitas, V.I., Ozsoy, I.B., 2009a. Micromechanical modeling of stress-induced phase transformations. part 1. thermodynamics and kinetics of coupled interface propagation and reorientation. Int. J. Plast. 25, 239–280.
Levitas, V.I., Ozsoy, I.B., 2009b. Micromechanical modeling of stress-induced phase transformations. part 2. computational algorithms and examples. Int. J. Plast. 25, 546–583.
Levitas, V.I., Preston, D.L., 2002a. Three-dimensional landau theory for multivariant stress-induced martensitic phase transformations, part i, austenite↔martensite. Phys. Rev. B 66, 1–9.
Levitas, V.I., Preston, D.L., 2002b. Three-dimensional landau theory for multivariant stress-induced martensitic phase transformations, part II multivariant phase transformations and stress space analysis. Phys. Rev. B. 66, 1–15.
Levitas, V.I., Preston, D.L., Lee, D.W., 2003. Three-dimensional landau theory for multivariant stress-induced martensitic phase transformations. III. alternative potentials, critical nuclei, kink solutions, and dislocation theory. Phys. Rev. B. 68, 134201.
Lexcellent, C., Leclercq, S., Gabry, B., Bourbon, G., 2000. The two way shape memory effect of shape memory alloys: an experimental study and a phenomenological model. Int. J. Plast. 16, 1155–1168.
Lim, T., McDowell, D.L., 2002. Cyclic thermomechanical behavior of a polycrystalline pseudoelastic shape memory alloy. J. Mech. Phys. Solids. 50, 651–676.
Mosler, J., Shchyglo, O., Montazer Hojjat, H., 2014. A novel homogenization method for phase field approaches based on partial rank-one relaxation. J. Mech. Phys. Solids. 68, 251–266.
Needleman, A., 1988. Material rate dependence and mesh sensitivity in localization problems. Comput. Methods in Appl. Mech. Eng. 67, 69–85.
Nemat-Nasser, S., Choi, J.Y., 2005. Strain rate dependence of deformation mechanisms in a ni-ti-cr shape-memory alloy. Acta Mater 53, 449–454.
Nemat-Nasser, S., Choi, J.Y., Guo, W.G., Isaacs, J.B., 2005. Very high strain-rate response of a NiTi shape-memory alloy. Mech. Mater. 37, 287–298.
Ozsoy, I.B., Babacan, N., 2016. Finite element simulations of microstructure evolution in stress-induced martensitic transformations. Int. J. Solids Struct. 81, 361–372.
Panico, M., Brinson, L.C., 2007. A three-dimensional phenomenological model for martensite reorientation in shape memory alloys. J. Mech. Phys. Solids. 55, 2491–2511.
Patoor, E., Berveiller, M., 1997. Micromechanical modelling of the thermomechanical behavior of shape memory alloys. In: Mechanics of Solids with Phase Changes. Springer, Vienna, pp. 121–188.
Roytburd, A.L., 1993. Elastic domains and polydomain phases in solids. Phase Trans. 45, 1–34.
Roytburd, A.L., Slutsker, J., 1997. Thermodynamic hysteresis of phase transformation in solids. Phys. B 233, 390–396.
Roytburd, A.L., Slutsker, J., 2001. Deformation of adaptive materials. part III: deformation of crystals with polytwin product phases. J. Mech. Phys. Solids 49, 1795–1822.
Saleeb, A.F., Padula, S.A., Kumar, A., 2011. A multi-axial, multimechanism based constitutive model for the comprehensive representation of the evolutionary response of SMAs under general thermomechanical loading conditions. Int. J. Plast. 27, 655–687.
Schneider, D., Tschukin, O., Choudhury, A., Selzer, M., Böhlke, T., Nestler, B., 2015. Phase-field elasticity model based on mechanical jump conditions. Comput. Mech. 55, 887–901.
Shaw, J.A., Kyriakides, S., 1995. Thermomechanical aspects of niti. J. Mech. Phys. Solids. 43, 1243–1281.
Shaw, J.A., Kyriakides, S., 1997a. Initiation and propagation of localized deformation in elasto-plastic strips under uniaxial tension. Int. J. Plast. 13, 837–871.
Shaw, J.A., Kyriakides, S., 1997b. On the nucleation and propagation of phase transformation fronts in a niti alloy. Acta Mater. 45, 683–700.
Siredey, N., Patoor, E., Berveiller, M., Eberhardt, A., 1999. Constitutive equations for polycrystalline thermoelastic shape memory alloys.: Part i. intragranular interactions and behavior of the grain. Int. J. Solids Struct. 36, 4289–4315.
Steinbach, I., Apel, M., 2006. Multi phase field model for solid state transformation with elastic strain. Phys. D. 217, 153–160.
Sun, Q.P., Zhao, H., Zhou, R., Saletti, D., Yin, H., 2012. Recent advances in spatiotemporal evolution of thermomechanical fields during the solid-solid phase transition. C. R. Mec. 340, 349–358.
Thamburaja, P., Anand, L., 2001. Polycrystalline shape-memory materials: effect of crystallographic. J. Mech. Phys. Solids. 49, 709–737.
Thomasová, M., Seiner, H., Sedlák, P., Frost, M., Sevčík, M., Szurman, I., Kocich, R., Drahokoupil, J., Sittner, P., Landa, M., 2017. Evolution of macroscopic elastic moduli of martensitic polycrystalline niti and niticu shape memory alloys with pseudoplastic straining. Acta Mater. 123, 146–156.
Tobushi, H., Tanaka, K., Hori, T., Sawada, T., Hattori, T., 1993. Pseudoelasticity of tini shape memory alloy: dependence on maximum strain and temperature. JSME Int. J., Ser. A. 36, 314–318.
Tůma, K., Stupkiewicz, S., 2016. Phase-field study of size-dependent morphology of austenite-twinned martensite interface in cualni. Int. J. Solids Struct. 97, 89–100.
Tse, K.K., Sun, Q.P., 2000. Some deformation features of polycrystalline superelastic niti shape memory alloy thin strips and wires under tension. Key Eng. Mater. 177, 455–460.
Umantsev, A., 2012. Field Theoretic Method in Phase Transformations. Lecture Notes in Physics 840. Springer, New York.
Wang, Y., Khachaturyan, A.G., 1997. Three-dimensional field model and computer modeling of martensitic transformations. Acta Mater 45, 759–773.
Wang, Y., Li, J., 2010. Phase field modeling of defects and deformation. Acta Mater. 58 (4), 1212–1235.
Wang, Y.U., Jin, Y.M., Khachaturyan, A.G., 2002. Phase field microelasticity theory and simulation of multiple voids and cracks in single crystals and polycrystals under applied stress. J. Appl. Phys. 91, 6435.
Zaki, W., Moumni, Z., 2007. A three-dimensional model of the thermomechanical behavior of shape memory alloys. J. Mech. Phys. Solids. 55, 2455–2490.
Zhang, X., Feng, P., He, Y., Yu, T., Sun, Q., 2010. Experimental study on rate dependence of macroscopic domain and stress hysteresis in niti shape memory alloy strips. Int. J. Mech. Sci. 52, 1660–1670.
Zhu, J., Gao, Y., Wang, D., Zhang, T.Y., Wang, Y., 2017. Taming martensitic transformation via concentration modulation at nanoscale. Acta Mater. 130, 196–207.

Please cite this article as: S.E. Esfahani et al., Microscale phase field modeling of the martensitic transformation during cyclic loading of NiTi single crystal, International Journal of Solids and Structures (2018), https://doi.org/10.1016/j.ijsolstr.2018.03.022